Molecular Cell

Article

The oxidoreductase PYROXD1 uses NAD(P)$^+$ as an antioxidant to sustain tRNA ligase activity in pre-tRNA splicing and unfolded protein response

Graphical abstract

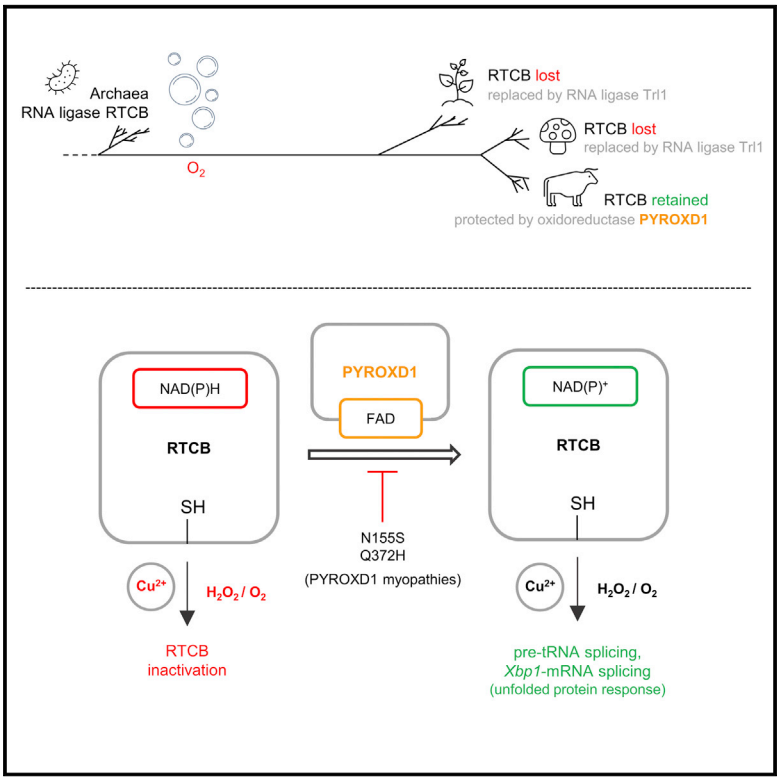

Highlights

- The RNA ligase RTCB is susceptible to copper-dependent oxidative inactivation
- The flavoprotein PYROXD1 uses NAD(P)$^+$ to safeguard mammalian RTCB against oxidation
- Depletion of PYROXD1 impairs pre-tRNA splicing and the unfolded protein response
- Myopathy-causing genetic variants of PYROXD1 fail to preserve the activity of RTCB

Authors

Igor Asanović, Emilia Strandback, Alena Kroupova, ..., Peter Macheroux, Stefan Weitzer, Javier Martinez

Correspondence

stefan.weitzer@meduniwien.ac.at (S.W.), javier.martinez@meduniwien.ac.at (J.M.)

In brief

How did enzymes from Earth's ancient anaerobic history, such as the RNA ligase RTCB, adapt to modern, aerobic environments? Asanovic et al. revealed an unexpected solution: RTCB co-evolved with a dedicated oxidoreductase, PYROXD1, which is linked to myopathies in humans, and paradoxically uses the principal prooxidative cofactor of the cell, NAD(P)$^+$, as the "private" antioxidative protector of RTCB.

Asanović et al., 2021, Molecular Cell *81*, 1–13
June 17, 2021
https://doi.org/10.1016/j.molcel.2021.04.007

CellPress

Please cite this article in press as: Asanović et al., The oxidoreductase PYROXD1 uses NAD(P)+ as an antioxidant to sustain tRNA ligase activity in pre-tRNA splicing and unfolded protein response, Molecular Cell (2021), https://doi.org/10.1016/j.molcel.2021.04.007

Molecular Cell

CellPress

Article

The oxidoreductase PYROXD1 uses NAD(P)+ as an antioxidant to sustain tRNA ligase activity in pre-tRNA splicing and unfolded protein response

Igor Asanović,[1] Emilia Strandback,[2,3,16] Alena Kroupova,[4,16] Djurdja Pasajlic,[1,16] Anton Meinhart,[5,16] Pai Tsung-Pin,[6,7,16] Nemanja Djokovic,[8,16] Dorothea Anrather,[9,16] Thomas Schuetz,[6,10] Marcin Józef Suskiewicz,[5,11] Sirelin Sillamaa,[12] Thomas Köcher,[13] Rebecca Beveridge,[5,14] Katarina Nikolic,[8] Alexander Schleiffer,[5,6] Martin Jinek,[4] Markus Hartl,[9] Tim Clausen,[5] Josef Penninger,[6,15] Peter Macheroux,[2] Stefan Weitzer,[1,*] and Javier Martinez[1,17,*]

[1]Max Perutz Labs, Medical University of Vienna, Vienna BioCenter (VBC), Dr. Bohr-Gasse 9/2, 1030 Vienna, Austria
[2]Institute of Biochemistry, Graz University of Technology, Petersgasse 12/2, 8010 Graz, Austria
[3]Department of Medical Biochemistry and Biophysics, Karolinska Institutet, 171 77 Stockholm, Sweden
[4]Department of Biochemistry, University of Zurich, Winterthurerstrasse 190, 8057 Zurich, Switzerland
[5]Research Institute of Molecular Pathology (IMP), Vienna BioCenter (VBC), Campus-Vienna-BioCenter 1, 1030 Vienna, Austria
[6]Institute of Molecular Biotechnology of the Austrian Academy of Sciences (IMBA), Vienna BioCenter (VBC), Dr. Bohr-Gasse 3, 1030 Vienna, Austria
[7]AnnJi Pharmaceutical, Taipei, Taiwan
[8]Department of Pharmaceutical Chemistry, Faculty of Pharmacy, University of Belgrade, Vojvode Stepe 450, 11221 Belgrade, Serbia
[9]Max Perutz Labs, University of Vienna, Vienna BioCenter (VBC), Dr. Bohr-Gasse 9, 1030 Vienna, Austria
[10]Department of Internal Medicine III (Cardiology and Angiology), Medical University of Innsbruck, Anichstraße 35, 6020 Innsbruck, Austria
[11]Sir William Dunn School of Pathology, University of Oxford, South Parks Road, OX1 3RE Oxford, UK
[12]Institute of Molecular and Cell Biology, University of Tartu, Riia 23, 51010 Tartu, Estonia
[13]Vienna BioCenter Core Facilities, Campus-Vienna-BioCenter 1, 1030 Vienna, Austria
[14]Department of Pure and Applied Chemistry, University of Strathclyde, 295 Cathedral Street, G1 1XL Glasgow, UK
[15]Department of Medical Genetics, Life Science Institute, University of British Columbia, C201 - 4500 Oak Street, V6H 3N1 Vancouver, BC, Canada
[16]These authors contributed equally
[17]Lead contact
*Correspondence: stefan.weitzer@meduniwien.ac.at (S.W.), javier.martinez@meduniwien.ac.at (J.M.)
https://doi.org/10.1016/j.molcel.2021.04.007

SUMMARY

The tRNA ligase complex (tRNA-LC) splices precursor tRNAs (pre-tRNA), and *Xbp1*-mRNA during the unfolded protein response (UPR). In aerobic conditions, a cysteine residue bound to two metal ions in its ancient, catalytic subunit RTCB could make the tRNA-LC susceptible to oxidative inactivation. Here, we confirm this hypothesis and reveal a co-evolutionary association between the tRNA-LC and PYROXD1, a conserved and essential oxidoreductase. We reveal that PYROXD1 preserves the activity of the mammalian tRNA-LC in pre-tRNA splicing and UPR. PYROXD1 binds the tRNA-LC in the presence of NAD(P)H and converts RTCB-bound NAD(P)H into NAD(P)+, a typical oxidative co-enzyme. However, NAD(P)+ here acts as an antioxidant and protects the tRNA-LC from oxidative inactivation, which is dependent on copper ions. Genetic variants of PYROXD1 that cause human myopathies only partially support tRNA-LC activity. Thus, we establish the tRNA-LC as an oxidation-sensitive metalloenzyme, safeguarded by the flavoprotein PYROXD1 through an unexpected redox mechanism.

INTRODUCTION

Post-transcriptional processing of RNA molecules guarantees the proper expression of the genome. During pre-mRNA splicing, the spliceosome removes introns and joins adjacent exons to generate mature, functional mRNAs (Will and Lührmann, 2011). A spliceosome-independent, non-canonical splicing pathway occurs in a subset of precursor tRNAs (pre-tRNAs) (Phizicky and Hopper, 2015; Schmidt and Matera, 2020) and in the mRNA encoding XBP1, the most conserved transcription factor required for the unfolded protein response (UPR) (Walter and Ron, 2011). Since all human pre-tRNAs decoding GTA, TAT, and CAA codons contain introns, non-canonical RNA splicing is essential for life (Gogakos et al., 2017; Schmidt and Matera, 2020).

Non-canonical RNA splicing entails two distinct enzymatic reactions: endonucleolytic cleavage of a single intron (Peebles

Please cite this article in press as: Asanović et al., The oxidoreductase PYROXD1 uses NAD(P)$^+$ as an antioxidant to sustain tRNA ligase activity in pre-tRNA splicing and unfolded protein response, Molecular Cell (2021), https://doi.org/10.1016/j.molcel.2021.04.007

et al., 1979; Yoshida et al., 2001) and ligation of exon halves. Both in pre-tRNA and *Xbp1*-mRNA splicing, the ligation reaction is catalyzed by the tRNA ligase complex (tRNA-LC) (Jurkin et al., 2014; Kosmaczewski et al., 2014; Lu et al., 2014; Popow et al., 2011) and its cofactor Archease, which uses guanosine triphosphate (GTP) to enable multiple catalytic cycles (Popow et al., 2014).

The catalytic subunit of the tRNA-LC is RTCB, a highly conserved enzyme that is present in all domains of life. In the anaerobic archaeon *Pyrococcus horikoshii*, RTCB is a binuclear metalloenzyme whose active site contains an essential cysteine residue coordinated to two metal ions (Desai et al., 2013; Englert et al., 2012). Such active sites are often highly sensitive to oxidative inactivation under aerobic conditions, in which they can encounter both molecular oxygen and partially reduced reactive oxygen species; the presence of an oxidized cysteine residue in the crystal structure of the aerobically purified archaeal RCTB (Banerjee et al., 2021), as well as the accumulation of tRNA exon halves in oxidatively stressed human cells (Hanada et al., 2013), suggests this may be the case for RTCB. To ensure catalysis, regulation, and stability, metalloenzymes in aerobic organisms have evolved multiple protective adaptations (Imlay et al., 2019). Adaptive mechanisms enabling RTCB to function in aerobic organisms, including humans, remain unknown.

Here, we reveal that RTCB, within the tRNA-LC, is inactivated by oxidative stress. The oxidoreductase PYROXD1 has co-evolved with the tRNA-LC to sustain its activity in human cells and in the mouse. PYROXD1 binds to RTCB and converts NAD(P)H into NAD(P)$^+$, which contrary to its established cellular role prevents copper ion-mediated oxidative inactivation of the tRNA-LC in our *in vitro* reconstituted system. Such a mechanism to protect metalloenzymes in aerobic organisms has not been reported. Finally, variants of PYROXD1 causing human myopathies display decreased enzymatic activity and fail to safeguard the tRNA-LC against oxidation.

RESULTS

The tRNA-LC requires the putative oxidoreductase PYROXD1 for activity *in vivo*

To identify factors potentially providing antioxidant protection to RTCB and maintaining its activity in aerobic *Eukarya*, we searched for proteins with the same species distribution as the subunits of the tRNA-LC in proteomes from all domains of life. This co-evolutionary analysis, using clusters of orthologous groups, revealed that in some aerobic organisms (e.g., plants, fungi) RTCB has been replaced by the non-homologous RNA ligase Trl1 (Greer et al., 1983), while in others (e.g., animals) it appears to have co-evolved with pyridine nucleotide-disulfide oxidoreductase domain-containing protein 1 (PYROXD1; Uniprot: Q8WU10), a putative oxidoreductase (Figure 1A).

PYROXD1 is an essential, conserved cytosolic protein, with variants causing an early-onset myopathy (N155S and Q372H) (O'Grady et al., 2016) and adult-onset limb-girdle-type muscular dystrophy (N155S and Y354C) (Sainio et al., 2019) in humans. PYROXD1 is homologous to textbook oxidoreductases, including NADH dehydrogenases and NADH oxidases (Figures 1B and S1A). Decreased cellular respiration in PYROXD1-deficient human cells (Lornage et al., 2019) and the ability of PYROXD1 to complement the loss of glutathione-reductase under oxidative stress in yeast (O'Grady et al., 2016) suggest that PYROXD1 also displays oxidoreductase activity.

To test whether PYROXD1 is required for tRNA-LC activity, we silenced its expression in human cells using RNA interference (RNAi). PYROXD1 depletion abrogated RNA ligation (Figure 1C) and pre-tRNA splicing in cell extracts (Figure S1B) and impaired the splicing of *Xbp1*-mRNA during UPR (Figure 1D). PYROXD1 depletion also resulted in the accumulation of tRNA fragments derived from intron-containing, tyrosine-GTA pre-tRNAs (Figure 1E), which also accumulate upon the depletion of RTCB (Figure S1C) and during oxidative stress (Hanada et al., 2013). Since the levels of the tRNA-LC subunits required for catalysis were not affected by PYROXD1 depletion (Figure S1D), we conclude that in cells, RTCB is inactivated in the absence of PYROXD1.

We found that PYROXD1 deletion is embryonically lethal in mice. Thus, to analyze PYROXD1 function *in vivo*, we generated a tamoxifen-inducible knockout (KO) in the heart (Figure S1E). Mice survived for 30 days after tamoxifen injection (Figure S1F), during which time we observed weakening of the cardiac ejection volume (Figure S1G), increased heart weight (Figure S1H), and progressive heart muscle fibrosis (Figure S1I), resulting in fatal heart failure. Deleting the *Pyroxd1* gene in the heart led to the accumulation of tyrosine-tRNA fragments (Figure 1F), confirming the functional interaction between PYROXD1 and the tRNA-LC *in vivo*. Our results show that the activity of the tRNA-LC in cells and *in vivo* depends upon the presence of PYROXD1.

PYROXD1 is a monomeric NAD(P)H-oxidizing flavoenzyme

To characterize PYROXD1 at the biochemical level, we produced recombinant human PYROXD1 in *Escherichia coli* and purified it to homogeneity by affinity capture and gel filtration (Figures S2A and S2B). PYROXD1 is loaded with the prosthetic group flavin adenine dinucleotide (FAD) (Figures 2A and S2C) and can be reduced by coenzymes NADPH and NADH (Figures 2B and S2D), which are converted to NADP$^+$ and NAD$^+$, respectively. In the N155S variant (Figure S2E), the rate of this reaction is ~25-fold lower (Figures 2C and S2D), indicating that the oxidation of NAD(P)H to NADP$^+$ by PYROXD1 is required for its physiological function. Reduced PYROXD1 could be re-oxidized by O_2 to enable multiple turnover (Figure S2F), but the rate of oxidation is limited by NAD(P)$^+$, which remains bound to PYROXD1 and hinders the access of O_2 to the enzymatic active site (Figure 2D; see Figure S3 for a detailed presentation of the underlying data). Model substrates containing disulfides could not substitute O_2 in this reaction, indicating that PYROXD1 has been incorrectly named (Q8WU10) as a disulfide reductase (Figure S3).

The crystal structure of PYROXD1 at 3.2 Å resolution (see Table 1 for structural statistics) revealed a typical flavoprotein architecture with three domains: the NAD(P)(H)-binding domain and the C-terminal domain, which are connected by a presumably non-structured loop with ambiguous electron density, and the FAD-binding domain, containing bound FAD (Figures 3A and 3B). The overall architecture of PYROXD1 is generally conserved when compared with homologous proteins (Figure 3C). However, the loop that contains catalytic and

Please cite this article in press as: Asanović et al., The oxidoreductase PYROXD1 uses NAD(P)$^+$ as an antioxidant to sustain tRNA ligase activity in pre-tRNA splicing and unfolded protein response, Molecular Cell (2021), https://doi.org/10.1016/j.molcel.2021.04.007

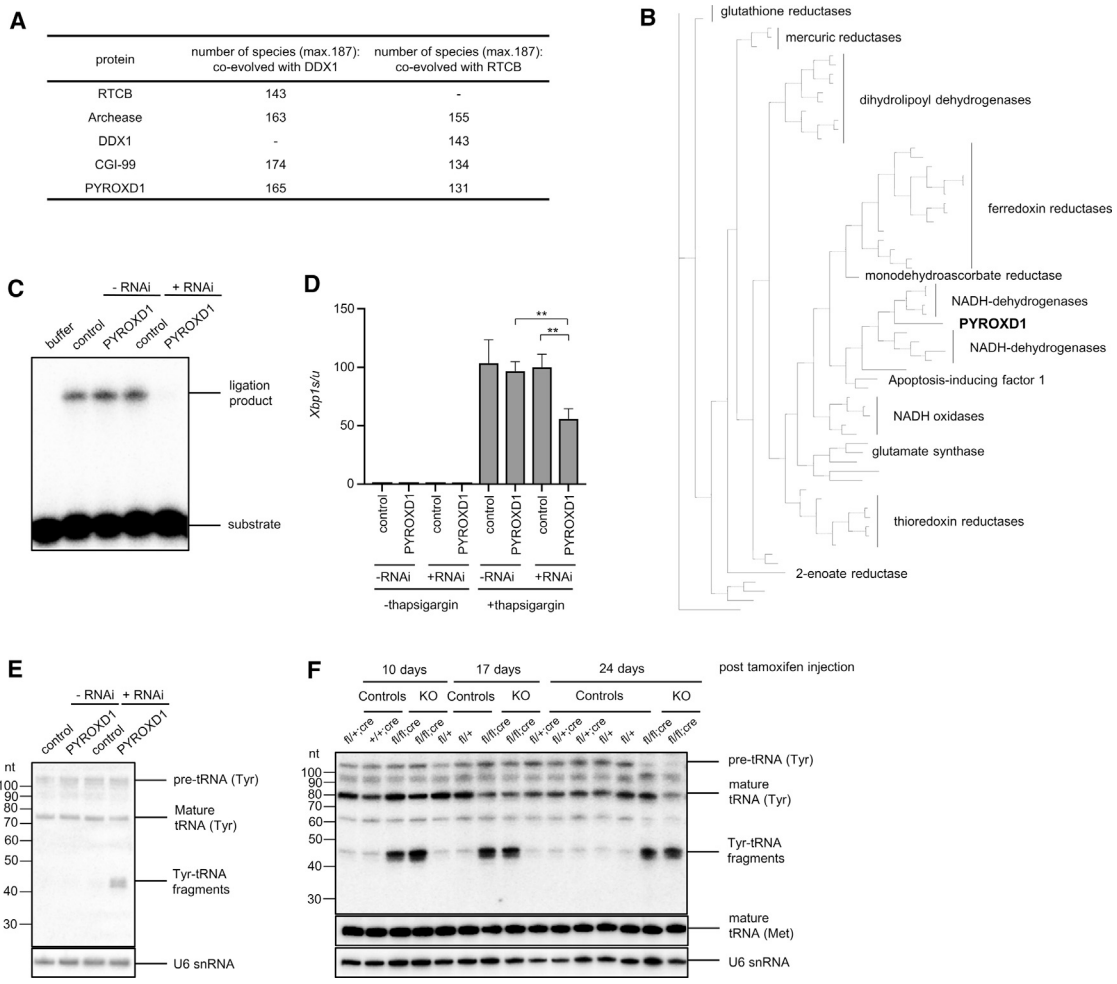

Figure 1. PYROXD1 is a putative oxidoreductase that co-evolved with the tRNA-LC and is essential for its activity in cells and *in vivo*

(A) Evolutionary clustering of orthologous groups in 187 eukaryotic species reveals co-evolution of PYROXD1 and tRNA ligase complex (tRNA-LC) subunits RTCB, DDX1, and CGI-99, and its cofactor Archease.

(B) Phylogenetic tree generated using the IQ-TREE web tool and the Pfam database seed group for Pyr_redox_2 domain, AIFM1, and PYROXD1, based on ClustalW multiple sequence alignments.

(C) HeLa cell lines expressing a doxycycline-inducible short hairpin against PYROXD1 were treated with doxycycline to trigger RNAi (+RNAi) or were left untreated (−RNAi). A cell line expressing a scramble short hairpin served as control. Cell extracts were incubated with an RNA duplex, 1 strand being internally radiolabeled (see Method details). Inter-strand ligation activity was monitored by denaturing gel electrophoresis.

(D) RNAi-mediated silencing of PYROXD1 in HeLa cells was induced as in (C), and cells were treated with thapsigargin to induce the unfolded protein response (UPR) or were left untreated. Relative mRNA levels of *Xbp1s* (spliced *Xbp1*) and *XBP1u* (unspliced *Xbp1*) were measured by quantitative polymerase chain reaction (qPCR) and shown as a ratio of *Xbp1s* to *Xbp1u*. Expression levels were normalized to *ACTB* mRNA levels and to the uninduced (−RNAi) and untreated cell lines. The experiment was done in independent triplicates, and values represent means ± SDs. **p $\leq$ 0.01 (unpaired Student's t test).

(E) RNA was isolated from cell lines in (C) and subjected to northern blot analysis using a probe complementary to the 5′ exon of Tyr-tRNA. U6 snRNA served as a loading control.

(F) Cre-recombinase was induced for the indicated times by tamoxifen treatment in mice leading to the knockout (KO) of the *Pyroxd1* gene in cardiomyocytes. RNA was isolated and subjected to northern blot analysis using a probe complementary to the 5′ exon of Tyr-tRNA. U6 snRNA and methionine tRNA served as controls. Control mice: fl/+;cre (*Pyroxd1*$^{fl/+}$;αMHC-MerCreMer), +/+;cre (*Pyroxd1*$^{+/+}$;αMHC-MerCreMer), fl/+ (*Pyroxd1*$^{fl/+}$). KO mice: fl/fl;cre (*Pyroxd1*$^{fl/fl}$; αMHC-MerCreMer). All mice were tamoxifen treated.

See also Figure S1.

substrate-binding motifs in homologs is displaced away from FAD in PYROXD1 (Figures 3C and S4A) and contains no known catalytic motifs, which is in line with the lack of disulfide reductase activity. The flavin ring is covered by the peptide stretch I131-D133 (Figures 3B and S4A) and the indole ring of W376 (Figure 3B). The replacement of W376 by alanine (Figure S2E) increased NAD(P)H oxidase activity ~4-fold (Figure S2F), showing that W376 further limits the access of O_2 to FAD. To model the structure of PYROXD1 in the NADP(H)-bound state, we combined two all-atom simulation approaches with

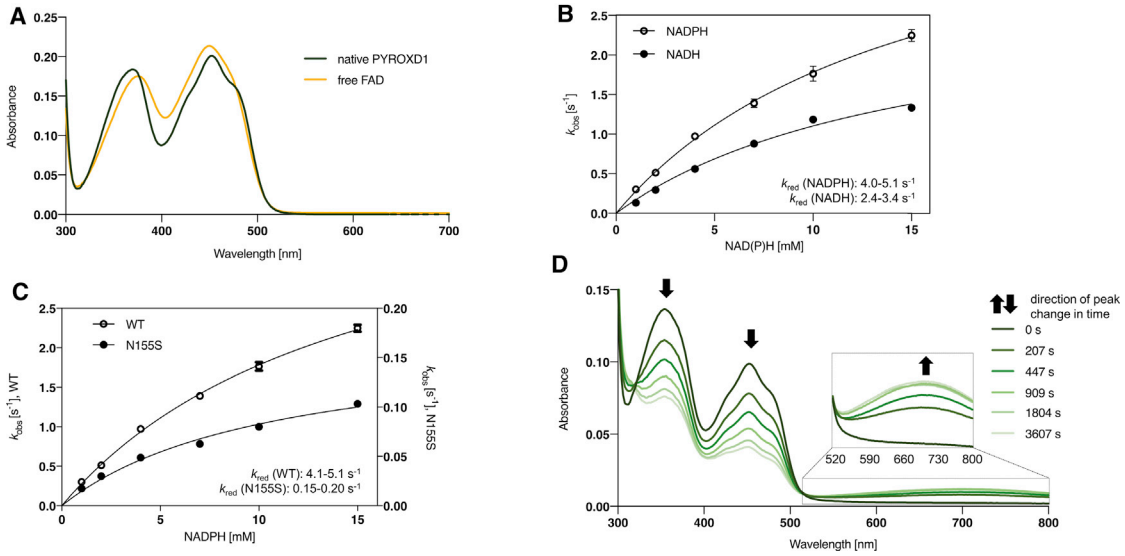

Figure 2. PYROXD1 is a flavoprotein with NAD(P)H oxidase activity

(A) Ultraviolet-visible spectra of native, yellow-colored recombinant PYROXD1 with FAD (green) and free FAD (yellow), liberated from PYROXD1 through denaturation by SDS (sodium dodecyl sulfate); the graph represents the typical spectra of a flavoprotein and a flavin cofactor (Macheroux, 1999), respectively, with peaks at ~370 nm and 450 nm and shoulder at 470 nm in the cofactor-bound state.

(B) Anaerobic pre-steady-state kinetics of the reductive rates of PYROXD1 by NAD(P)H. Recombinant PYROXD1 at a fixed concentration was mixed with increasing amounts of NADPH, followed by the measurement of absorbance drop rates at 451 nm (FAD reduction).

(C) Anaerobic pre-steady-state kinetics were performed as in (B), using NADPH as electron donor, for recombinant wild type (WT) and the disease-causing variant N155S. In both (B) and (C), the results are presented as mean values of the corresponding technical triplicate with standard deviation at $\sigma = 0.05$.

(D) Recombinant PYROXD1 was mixed with NADPH under anaerobic conditions and spectra were recorded at regular time intervals. Black arrows indicate the direction of peak changes during the reduction. The broad peak at wavelengths >500 nm corresponds to the charge-transfer complex (CTC), formed between NADP$^+$ and the reduced FAD within PYROXD1, also visible through the color change from yellow to blue (see Figure S3 for the characterization of the CTC and its effects on the kinetics of PYROXD1 oxidation).

See also Figure S2.

ensemble docking (see Figure S5 for a detailed presentation of the model). The model predicts that N155 is involved in positioning NAD(P)H (Figure 3D) in the active site formed upon a conformational change in PYROXD1 required for nucleotide binding (Figure S4B); this explains the lower reductive rate in the N155S variant (Figure 2C).

Recombinant PYROXD1 exists predominantly as a monomer (Figure 3E). H410 in monomeric PYROXD1 occupies a similar geometric position to catalytic histidine residues in dimeric, homologous proteins (Figure S4C), and its replacement with alanine (H410A) impairs activity (Figures S2E and S2F). Thus, H410 makes PYROXD1 unique among its family members (Argyrou and Blanchard, 2004) by enabling enzymatic activity as a monomer (Figures S4D and S4E) without the need to homodimerize (see Figure S6 for further evidence of this claim).

The tRNA-LC is redox regulated

While PYROXD1 is essential for tRNA-LC activity in cells, both recombinant tRNA-LC and RTCB purified from insect cells are active in the absence of PYROXD1 (see below). This suggests that PYROXD1 maintains rather than promotes the activity of the tRNA-LC, presumably by protecting the active site of RTCB (Figure 4A) from oxidative inactivation. To investigate whether the tRNA-LC is indeed sensitive to oxidative stress, we treated HeLa cells with the increasing concentrations of the oxidative stressors menadione and H_2O_2, and monitored RNA ligation in a pre-tRNA splicing assay. The ligation of tRNA exon halves was specifically abrogated, since the activity of the tRNA splicing endonuclease (TSEN) complex, which removes the single tRNA intron (Peebles et al., 1979), remained intact (Figures 4B and S7A). Using pre-tRNA splicing, interstrand ligation, and northern blot analysis, we further demonstrated that the oxidative inactivation of the tRNA-LC was dose dependent (Figures 4B and S7A–S7E), reversible after the removal of the stressing agent (Figure 4C), and rescued by the antioxidant *N*-acetylcysteine (NAC), which boosted the activity of the tRNA-LC even without treatment with oxidants (i.e., under background oxidative stress) (Figure 4D). These results indicate that the redox sensitivity of the tRNA-LC could be used for reversible, malleable regulation.

To reconstitute the sensitivity of the tRNA-LC to oxidation *in vitro*, we incubated either human tRNA-LC (Figure S7F) or RTCB (Figure S7G) recombinant proteins, with cofactor Archease and increasing concentrations of H_2O_2. RNA ligation activity was abrogated by H_2O_2 in both cases (Figure 4E). Prior oxidative treatment of the tRNA-LC, but not Archease, abrogated RNA ligation (Figure S7H). These results confirmed our original hypothesis that RTCB is sensitive to oxidative inactivation, both alone or within the tRNA-LC. The reducing agent TCEP prevented the loss of RNA ligation activity by H_2O_2 (Figure S7I).

Please cite this article in press as: Asanović et al., The oxidoreductase PYROXD1 uses NAD(P)$^+$ as an antioxidant to sustain tRNA ligase activity in pre-tRNA splicing and unfolded protein response, Molecular Cell (2021), https://doi.org/10.1016/j.molcel.2021.04.007

Table 1. Table of structural statistics

Data statistics	
Space group	$P3_112$
a, b, c (Å)	101.23, 101.23, 143.45
Resolution	20–3.2 (3.28–3.2)
R_{meas} (%)	11.0 (186.4)
$CC_{½}$	99.8 (56.1)
I/σ(I)	13.58 (1.24)
No. unique reflections (anomalous)	26,957 (1,997)
Completeness (%)	99.3 (99.7)
Redundancy	5.5 (5.7)
Refinement statistics	
Resolution	20–3.2 (3.314–3.2)
No. unique reflections (non-anomalous)	14,003 (1,393)
Completeness (%)	99.21 (99.64)
R_{work}/R_{free} (%)	0.217/0.234
No. atoms	
Protein	3,327
Ligand	53
B-factor	
Protein	123.90
Ligand	103.60
Rmsd	
Bond lengths (Å)	0.003
Bond angles (°)	0.56

Data and refinement statistics related to the structure of PYROXD1 with FAD, deposited under PDB: 6ZK7.

Co-incubation of the tRNA-LC (Figure 4F) or RTCB (Figure S7J) with H_2O_2 and dimedone, which labels cysteine sulfenic acid *in situ*, uncovered the correlation between oxidation of cysteine(s) to sulfenic acid in RTCB and inactivation of the tRNA-LC. However, since the loss of the enzymatic activity occurs at slightly higher concentrations of H_2O_2 than the dimedone signal, we speculate that the tRNA-LC inactivation observed in our *in vitro* system could be to a significant extent driven by the further oxidation to sulfinic or sulfonic acid. Under higher concentrations of H_2O_2, sulfenic acids also accumulate in the RNA helicase subunit DDX1 (Figure 4F), which may fine-tune the regulation of RTCB.

Oxidative inactivation of the tRNA-LC can thus be reconstituted *in vitro*. However, the relatively high concentrations of H_2O_2 required for inactivation suggest that the *in vitro* system may be lacking a sensitizing factor or factors.

Cu^{2+} is critical for redox regulation of the tRNA-LC *in vitro*

We hypothesized that the sensitivity of the tRNA-LC toward oxidation could depend on at least one metal ion in the active site. Since the metal chelator imidazole was used during its purification, we reasoned that the recombinant tRNA-LC may not be fully loaded with native metals and that redox regulation occurs only upon the binding of trace metal ions from the reaction buffer. To test this, we pre-treated the reaction buffer with the metal ion-chelating resin Chelex 100, followed by supplementation with a series of potentially regulatory metals, and with Mg to enable tRNA-LC activity. The sensitivity of the tRNA-LC to oxidative inactivation was largely reduced in the buffer where trace metals had been removed by pre-treatment with Chelex 100 (Figure 4G). Supplementation of this reaction buffer with nanomolar concentrations of Cu^{2+}, but not other metal ions, fully restored the sensitivity of the tRNA-LC to oxidative inactivation by H_2O_2 (Figure 4H). Cu^{2+} sensitized the tRNA-LC to oxidation in near-equimolar concentrations, but it did not affect the activity of the tRNA-LC in the absence of H_2O_2 (Figure S7K; corresponding quantification in the lower panel). Accumulation of dimedone-labeled sulfenic acids in RTCB, upon incubation of the tRNA-LC with H_2O_2, was similarly boosted by nanomolar Cu^{2+} concentrations (Figure S7L). Thus, we conclude that under the conditions of our reconstituted system, catalytic amounts of free Cu are critical for the regulation of the tRNA-LC, but not for its activity or stability.

PYROXD1 and the tRNA-LC interact in the presence of NAD(P)H

We tested whether a physical interaction could mediate the protective function of PYROXD1 toward the tRNA-LC. Co-immunoprecipitation revealed that PYROXD1 and the tRNA-LC interact, but only in the presence of NAD(P)(H) (Figure 5A), an effect not mimicked by ATP, GTP, FAD, H_2O_2 or ubiquinone-1. The reduced nucleotides NADH and NADPH were equally capable of enabling the interaction, but NAD^+ and $NADP^+$ were less efficient (Figure 5A). Mass spectrometry analysis of co-immunoprecipitates from cells expressing FLAG-PYROXD1 detected RTCB and the other tRNA-LC subunits as the main interactors of PYROXD1 upon addition of $NADP^+$ (Figure 5B) and NADPH (Figures S8A and S8B) to the cell extracts. We reproduced these findings *in vitro* by pulling down recombinant PYROXD1 with StrepII-GFP-RTCB in the presence of NAD(P)H (Figure 5C); here, $NAD(P)^+$ did not mediate binding. The apparent $NAD(P)^+$-mediated interaction in extracts (Figures 5A and 5B) could occur due to a partial conversion of $NAD(P)^+$ into NAD(P)H. Thus, PYROXD1 interacts with the tRNA-LC, mainly in the presence of NAD(P)H.

$NAD(P)^+$ and NAD(P)H control the sensitivity of the tRNA-LC to oxidation

To investigate the potential role of nicotinamide dinucleotides in redox regulation of the tRNA-LC, we added NADPH and $NADP^+$ to our *in vitro* reconstituted system (see Figure 4E). Addition of the reduced nucleotides NAD(P)H increased tRNA-LC sensitivity to oxidation by H_2O_2, while the addition of $NAD(P)^+$ made the tRNA-LC more resistant (Figures 6A and S9A), suggesting that NAD(P)(H) binds the tRNA-LC and largely alters its redox properties. Incubation of recombinant tRNA-LC with streptavidin magnetic beads coated with biotinylated NAD^+ enabled pulling down RTCB and DDX1 subunits of the tRNA-LC, and this effect was abolished when NADPH, $NADP^+$, NADH, or NAD^+ were used as competitors (Figure S9B). Thus, like PYROXD1, the tRNA-LC interacts with NADP(H) and NAD(H).

NADPH triggers Fenton reactions in chemical systems, resulting in the production of reactive oxygen species (ROS) through

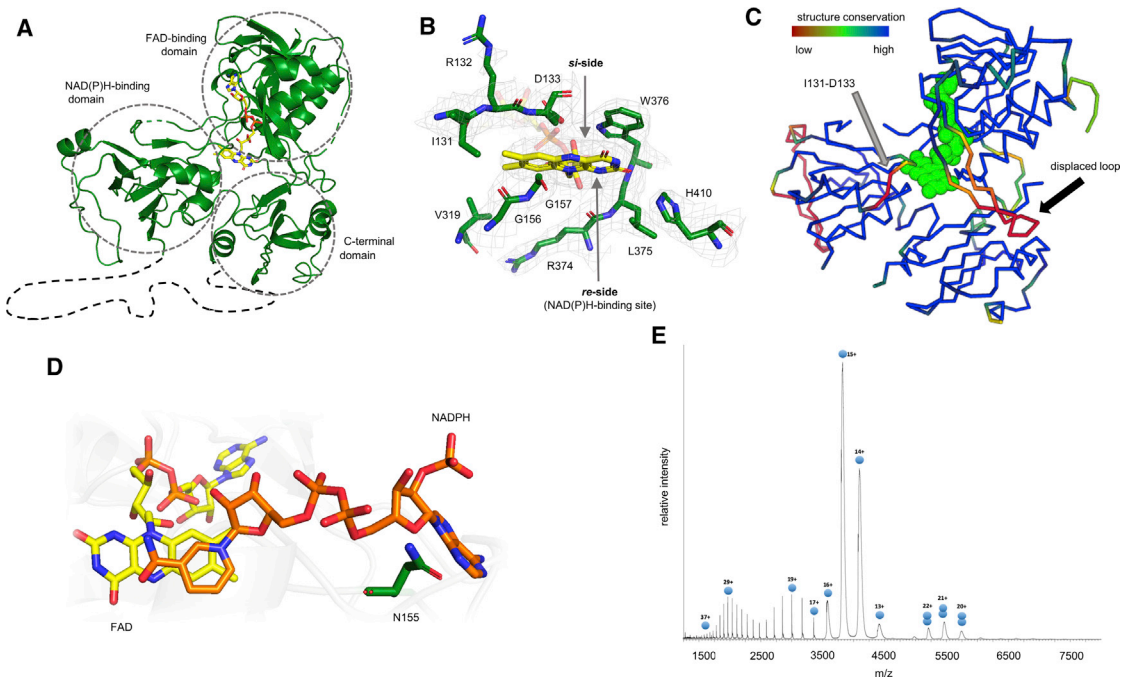

Figure 3. The crystal structure of PYROXD1 reveals a unique monomeric active site and the NAD(P)H positioning role of the disease-affected residue N155

(A) The overall domain structure of PYROXD1 includes the FAD-binding domain (FAD shown in yellow), the NAD(P)H-binding domain, and the C-terminal domain (see Table 1 for detailed information on the structure). The NADPH-binding domain and the C-terminal domain are connected by an unresolved, presumably unstructured loop.

(B) Surrounding of the flavin isoalloxazine ring: the *re*-side includes the catalytically essential H410 and comprises the position where nicotinamide nucleotide is expected to bind; the *si*-side has no cysteine residues and appears covered by W376 and the peptide backbone of I131, R132, and D133. FAD (yellow), amino acid residues (green; N_2: blue, O_2: red). 3Fo-2Fc omit electron density is contoured at 1σ around the isoalloxazine ring and surrounding residues (light gray).

(C) The PYROXD1 structure was uploaded to the Dali server and compared to the structures of 30 homologous proteins to identify unique regions. Blue: regions in PYROXD1 that are structurally conserved compared to homologs; red: structurally unique regions in PYROXD1; green spheres: FAD; arrows point to structurally unique polypeptide stretches in the PYROXD1 active site.

(D) NADPH was modeled into the structure of PYROXD1 using all atom simulations and ensemble docking. FAD (yellow), NADPH (orange), and N155 residue (green) (see Figure S5 for a detailed presentation of the modeling approaches and results).

(E) Recombinant PYROXD1 was analyzed using native mass spectrometry. Schematically labeled peaks correspond to different charge states (indicated above the peaks) of the most abundant oligomeric forms of PYROXD1: monomer (single blue circle), dimer (double blue circle); *m/z*, mass-to-charge ratio (see Figure S6 for more details on the dynamics of the oligomeric states of PYROXD1).

See also Figure S4.

direct reactions with Cu^{2+} ions (Rowley and Halliwell, 1985). However, a mode of direct redox regulation of a metalloenzyme with NAD(P)$^+$ as a protector and NAD(P)H as a sensitizer, as shown in our reconstitution experiments, has not been observed in a biochemical context. To test whether a Fenton reaction mediates nucleotide effects on the tRNA-LC, we included bathocuproinedisulfonic acid (BCS), a chelator of the Fenton intermediate Cu^+, into the reconstitution system. BCS turned the tRNA-LC resistant to oxidative inactivation and abolished the effects of the nucleotides, showing that the Fenton reaction with Cu^{2+} ions plays a crucial role both in the sensitivity of the tRNA-LC to oxidation and in its modulation by NAD(P)(H) *in vitro* (Figure 6B).

PYROXD1 uses NAD(P)$^+$ to prevent oxidative inactivation of the tRNA-LC *in vitro*

To finally test whether PYROXD1 protects the tRNA-LC from oxidative inactivation *in vitro*, we added PYROXD1 to our reconstituted system composed of tRNA-LC, Archease, NADPH, H_2O_2, and a reaction buffer containing trace metals, including Cu. Under these conditions, PYROXD1 largely prevented the inactivation of the tRNA-LC (Figure 6C). The protective effect was less pronounced with the disease variant N155S (Figure 6C), which oxidizes NADPH to NADP$^+$ at a lower rate (Figures 2C, 3D, S2D, and S2F). When variants Q372H (causing myopathy) and H410A (designed based on the crystal structure) were used (Figure S2E), the protective effect on the tRNA-LC was reduced proportionally to the impairment in their oxidoreductase activities (Figures S2F and S9C). Similarly, the tRNA-LC was more efficiently rescued by purified monomeric than the less active dimeric form of PYROXD1 (Figures S4D, S4E, and S9D). Heat-denatured PYROXD1 did not protect the tRNA-LC against oxidative inactivation (Figure S9E). In addition, PYROXD1 could prevent, but not rescue, the oxidative inactivation of the tRNA-LC, confirming that PYROXD1 acts upstream in the inactivation cascade in our reconstituted system (Figure S9F). These data

Please cite this article in press as: Asanović et al., The oxidoreductase PYROXD1 uses NAD(P)$^+$ as an antioxidant to sustain tRNA ligase activity in pre-tRNA splicing and unfolded protein response, Molecular Cell (2021), https://doi.org/10.1016/j.molcel.2021.04.007

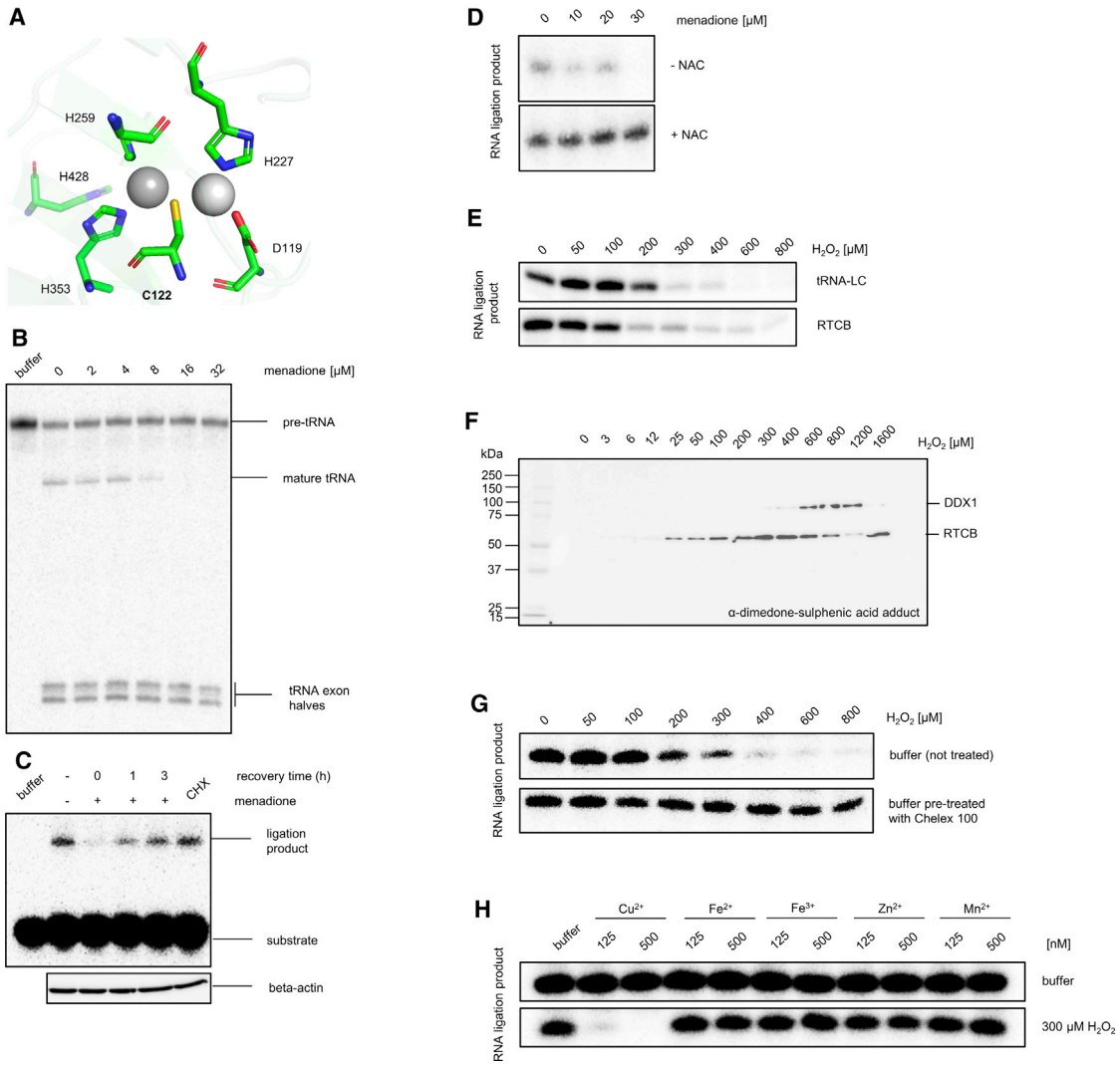

Figure 4. The tRNA ligase complex is inhibited by oxidative stress and boosted by the antioxidant *N*-acetylcysteine (NAC), and its oxidative inactivation can be reconstituted *in vitro* in the presence of catalytic amounts of available Cu ions

(A) A homology-based model of RTCB was generated using the Swiss-model tool based on PDB: 4dwr (RTCB from *Pyrococcus horikoshii*; Englert et al., 2012). Shown is the predicted RTCB active site containing the essential cysteine residue C122, coordinated to 2 metal ions.

(B) HeLa cells were treated with the indicated concentrations of menadione, and cell extracts were assayed for pre-tRNA splicing by incubation with an internally radiolabeled, intron-containing yeast pre-tRNA^{Phe}. Pre-tRNA processing was monitored by denaturing gel electrophoresis.

(C) HeLa cells were treated with menadione, and cells were recovered in the presence of cycloheximide to inhibit *de novo* protein synthesis. Samples were taken at indicated time points (recovery time) and assayed for inter-strand ligation activity (top). CHX, cycloheximide-only cell treatment, without prior menadione addition. Western blot analysis probing for β-actin confirmed equal protein concentration in all of the samples (bottom).

(D) HeLa cells were treated with menadione at the indicated concentrations for 1 h in the presence or absence of NAC. Cell extracts were assayed for inter-strand ligation activity as in (C).

(E) Recombinant tRNA-LC or RTCB and Archease were incubated with increasing concentrations of H_2O_2. RNA ligation was assayed by circularization of a radiolabeled, single-stranded oligonucleotide and monitored by denaturing gel electrophoresis.

(F) Recombinant tRNA-LC was incubated with the increasing concentrations of H_2O_2 in the presence of the sulfenic-acid labeling reagent dimedone. Proteins were analyzed by SDS-PAGE followed by western blot detection of cysteine-sulfenic acid adducts.

(G) Trace metal-free reaction buffer was prepared by pre-treatment with the chelating resin Chelex 100. Then, tRNA-LC and Archease were incubated with increasing concentrations of H_2O_2 in both non-treated and Chelex-treated buffer, and the ligation activity was measured as described in (E).

(H) A reaction buffer free of trace metals was prepared as in (G). Then, the recombinant tRNA-LC and Archease were incubated with different biologically relevant metal ions and H_2O_2, and RNA ligation was monitored as described in (E).

See also Figure S7.

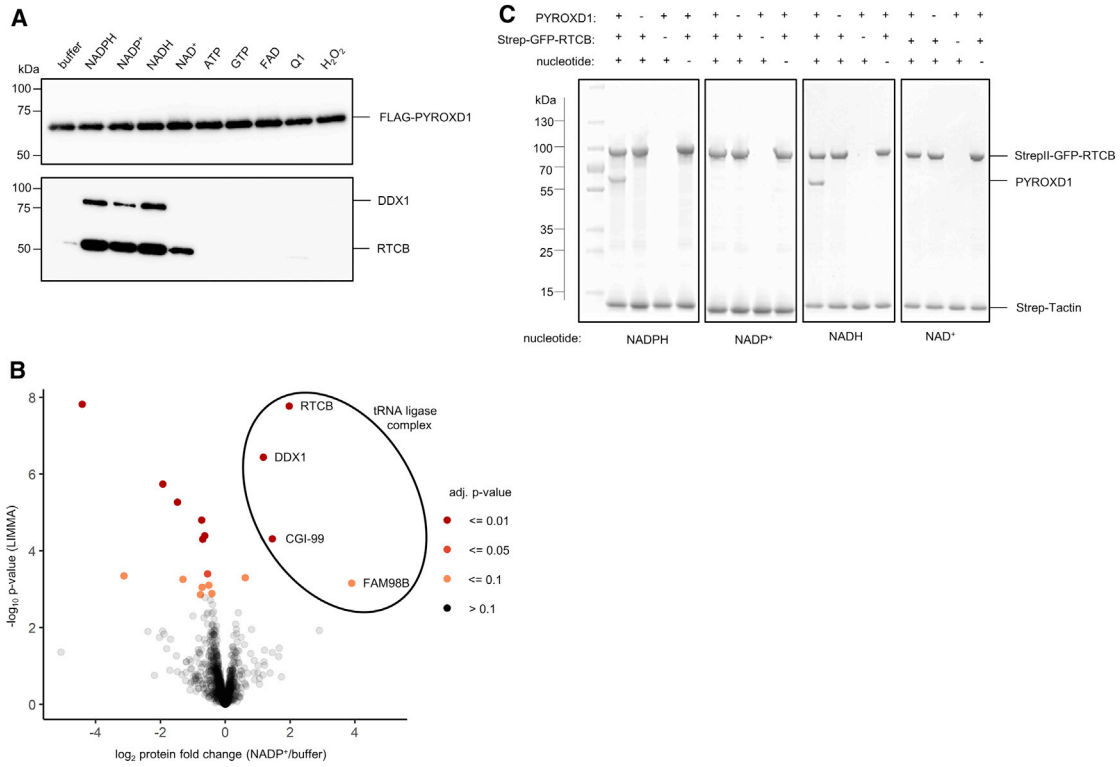

Figure 5. PYROXD1 interacts with the tRNA-LC in presence of NAD(P)H

(A) Anti-FLAG immunoprecipitation was performed using cell extracts derived from a cell line expressing doxycycline-inducible FLAG-PYROXD1, without addition (buffer) or with addition of the indicated compounds. FLAG-PYROXD1 and co-purified tRNA-LC subunits RTCB and DDX1 were detected by western blotting.

(B) FLAG-PYROXD1 was immunoprecipitated from cell extracts in independent triplicate experiments in the absence (buffer) or presence of NADP$^+$, followed by mass spectrometry analysis.

(C) Recombinant PYROXD1 and StrepII-GFP-RTCB were incubated in a buffer with or without NAD(P)(H), followed by pull-down using Strep-Tactin beads. Beads were washed and bound proteins were analyzed by SDS-PAGE and Coomassie blue staining.

See also Figure S8.

demonstrate that the catalytic activity of PYROXD1 is required to preserve the function of the tRNA-LC in oxidizing environments.

DISCUSSION

We have shown that PYROXD1 protects the tRNA-LC and its catalytic subunit RTCB, an archaic protein that has been preserved only in those aerobic species in which co-evolution with PYROXD1 had taken place; their co-evolution is also reflected in the modern-day context through the codependency of PYROXD1 and RTCB in cancer cell lines (DepMap: PYROXD1). Consistent with our reconstitution experiments, we proposed that the Cu ion in the active site of RTCB could make a cysteine residue more prone to oxidation and behaves as a local generator of ROS, such as HO$^{\cdot}$ (hydroxyl) and HOO$^{\cdot}$ (hydroperoxyl) radicals, through a Fenton reaction (Figure 6D).

In line with the RNA-enzyme-metabolite (REM) concept (Hentze and Preiss, 2010), we suggest that the RNA, ATP, or GTP binding sites of RTCB (Englert et al., 2012) can accommodate NAD(P)$^+$ or NAD(P)H, which act as a suppressor or stimulator, respectively, of Cu-mediated oxidative inactivation (Figure 6A). We thus believe that the effects of oxygen and ROS, as well as of Cu and NAD(P)(H), are a direct consequence of the chemical nature of RTCB, which makes it prone to oxidative inactivation. However, co-evolution of PYROXD1 allowed aerobic organisms to turn this hazardous inactivating reaction into a controlled process used to regulate the tRNA-LC activity (see below).

PYROXD1 oxidizes NAD(P)H to NAD(P)$^+$ with tightly controlled kinetics, reducing one molecule of O_2 into H_2O_2 per turnover (Figure S3). This reaction is a double-edged sword: while it ensures that the protecting, oxidized nucleotide NAD(P)$^+$ is bound to the RTCB active site, it also produces undesirable H_2O_2 in its vicinity, as illustrated by the gain-of-function variant W376A, which not only fails to protect the tRNA-LC against oxidation but rather inhibits its activity due to a higher rate of H_2O_2 production (Figure S9G). Thus, PYROXD1 must operate within a narrow activity range, as evidenced by the failure of both loss- and gain-of-function variants to protect the tRNA-LC. Furthermore, we believe that PYROXD1 evolved to bind to the tRNA-LC only in the presence of NAD(P)H and dissociates upon the generation of NAD(P)$^+$ (Figure 5C), precisely to avoid

Please cite this article in press as: Asanović et al., The oxidoreductase PYROXD1 uses NAD(P)$^+$ as an antioxidant to sustain tRNA ligase activity in pre-tRNA splicing and unfolded protein response, Molecular Cell (2021), https://doi.org/10.1016/j.molcel.2021.04.007

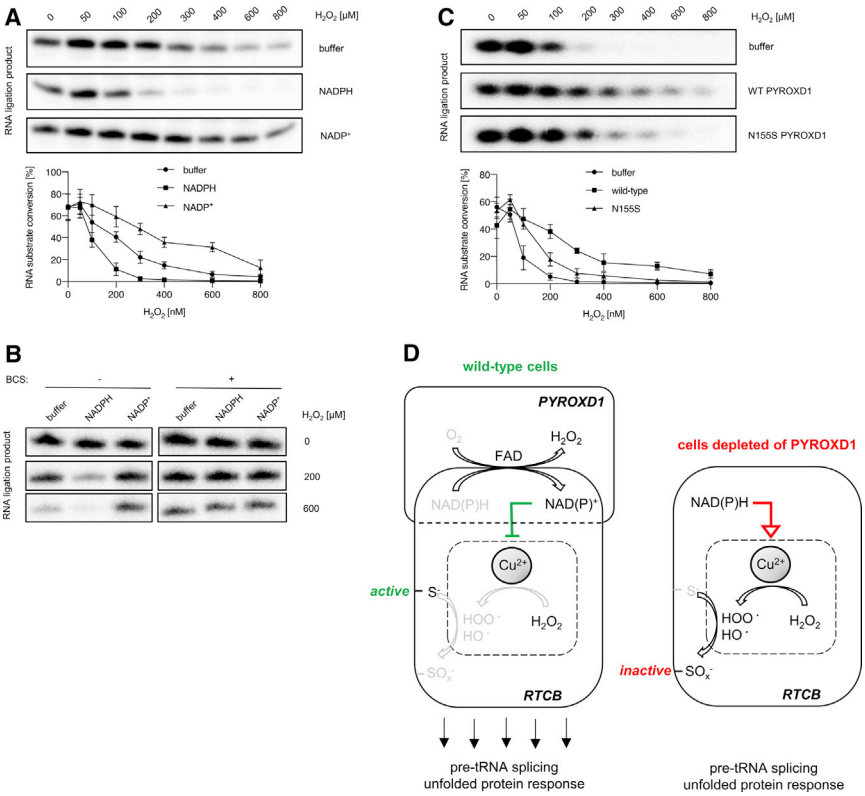

Figure 6. *In vitro* reconstituted system indicates that PYROXD1 prevents the oxidative inactivation of the tRNA-LC through the oxidation of NAD(P)H into NADP$^+$

(A) Top: recombinant tRNA-LC and Archease were incubated with NADP(H) and increasing concentrations of H_2O_2. RNA ligation was assayed by circularization of a radiolabeled, single-stranded oligoribonucleotide and monitored by denaturing gel electrophoresis (see Method details). A representative result is shown. Bottom: quantification of independent quadruplicate experiments: RNA substrate conversion (as mean values ± SEMs at 95% confidence intervals) was plotted against H_2O_2 concentration.

(B) Recombinant tRNA-LC and Archease were incubated with NADP(H) and 2 concentrations of H_2O_2, in the absence or presence of the Cu chelator BCS. RNA ligation was assayed as in (A).

(C) Top: recombinant tRNA-LC and Archease were incubated with recombinant PYROXD1 (WT or N155S), NADPH, and increasing concentrations of H_2O_2. RNA ligation was assayed as in (A). A representative result is shown. Bottom: quantification of independent triplicate experiments: RNA substrate conversion (as mean values ± SEMs at 95% confidence intervals) was plotted against H_2O_2 concentration.

(D) Model depicting the protective function that PYROXD1 exerts on the tRNA-LC. Designation "x" in the oxidized form of RTCB emphasizes the uncertainty of the contributions of sulfenic, sulfinic, and sulfonic acid forms (x = 1, 2, and 3, respectively) to the inactivation of the tRNA-LC under various oxidizing conditions.

See also Figure S9.

multiple catalytic cycles that would lead to local accumulation of H_2O_2.

However, besides O_2, an additional, thus far unknown electron acceptor for PYROXD1 may exist, whose reduced form may not suppress tRNA-LC activity. This idea is consistent with PYROXD1's complementing the loss of glutathione reductase under oxidative stress conditions in yeast (O'Grady et al., 2016), which suggests a more general antioxidative function. PYROXD1 reduces ubiquinone-1 (Figure S3); nonetheless, this is an unspecific and non-physiological substrate. Also, PYROXD1 does not have an integral membrane domain, and most natural quinone or quinoid compounds are membrane bound. The identification of additional, *in vivo* relevant electron acceptors for PYROXD1 could shed light on alternative cellular functions.

While NAD$^+$ enables SIRT enzymes to deacetylate and activate glucose-6-phosphate dehydrogenase, ultimately increasing cellular production of antioxidative NADPH (Xiao et al., 2018), the direct use of NAD(P)$^+$ as an antioxidant as indicated by our reconstitution experiments is novel in redox biology. This mechanism adds to the repertoire of strategies evolved to preserve the activity of metalloenzymes in aerobic environments (Imlay et al., 2019) and presumably establishes the tRNA-LC as one of the few human proteins dependent on Cu. How this regulation occurs at the chemical level and whether this mechanism is unique to the tRNA-LC or more universally applicable to aerobic Cu-binding proteins remains to be uncovered.

The reversibility and plasticity of the oxidative inactivation of the tRNA-LC (Figures 4B–4D) and the specificity for the rare trace element Cu (Figure 4H) suggest that the redox sensitivity of the tRNA-LC has a regulatory function and is not a mere evolutionary relic. Redox protection of the tRNA-LC by PYROXD1 could be critical during the UPR, in which the tRNA-LC displays a pro-survival function (Hetz, 2012; Lin et al., 2007) serving as a molecular switch during oxidative stress coupled to endoplasmic reticulum (ER) stress. The UPR is important in the development and maintenance of skeletal muscle, a tissue with an elaborate ER structure (Bohnert et al., 2018). Thus, our characterization of PYROXD1 disease-causing variants provides a potential link between myopathies and inactivation of the tRNA-LC, which is consistent with PYROXD1 being found in proximity to skeletal muscle ER (O'Grady et al., 2016), the tRNA-LC being proximal to the ER in HeLa cells (Lu et al., 2014) and the tRNA-LC interacting with IRE1 at the ER membrane (Acosta-Alvear et al., 2018). While disease-causing variants of PYROXD1 fail to protect the tRNA-LC, the mechanistic link between the tRNA-LC, the ability of PYROXD1 to act as a metalloenzyme protector, and muscle malfunction merits further characterization.

Please cite this article in press as: Asanović et al., The oxidoreductase PYROXD1 uses NAD(P)$^+$ as an antioxidant to sustain tRNA ligase activity in pre-tRNA splicing and unfolded protein response, Molecular Cell (2021), https://doi.org/10.1016/j.molcel.2021.04.007

Limitations of the study

Our *in vitro* reconstitution experiments rely on H_2O_2 to oxidatively inactivate the tRNA-LC. However, the tRNA-LC in cells and in the mouse heart is inactivated upon 6 days of PYROXD1 absence without the addition of exogenous H_2O_2. This suggests that the prolonged exposure of the tRNA-LC to O_2 could be sufficient to inactivate it, a hypothesis that is consistent with the evolutionary perspective of the phylogenetic clustering. To test this *in vitro*, we exposed the tRNA-LC and Archease to an oxygenic atmosphere for 6 days. The tRNA-LC lost activity, in a manner preventable by the reducing agent tris(2-carboxyethyl)phosphine) (TCEP) (Figure S9H). This result strongly suggests loss of activity through oxidative inactivation, rather than proteolytic degradation or unfolding. Protection of the tRNA-LC from O_2 by the PYROXD1:NAD(P)H system is nevertheless difficult to fully reconstitute since NAD(P)H and PYROXD1 are not stable enough for such long-term *in vitro* experiments. The next challenge consists in identifying metal ions natively bound to the tRNA-LC. To unambiguously identify the metal ions in the tRNA-LC in human cells, we should be able to purify sufficient amounts of the native complex from human cells to perform induced coupled plasma measurements, which is currently a very difficult task. The final challenge is obtaining causative evidence supporting the robust correlative relationships between the presence of H_2O_2, Cu, and NAD(P)H, and the inactivation of the tRNA-LC through cysteine oxidation to sulfenic acid. To overcome this, we need to generate RTCB mutants that have altered affinities for NAD(P)H and/or Cu; ultimately, we would aim to obtain mutant versions of RTCB that retain activity but are resistant to oxidative inactivation. If successful, we could use CRISPR-Cas9 to generate cell lines or a mouse model expressing such mutants and use them to study the physiological purpose of regulating tRNA-LC. This is a difficult task for two reasons: (1) C122 is catalytically essential, and mutagenesis could abrogate the regulation together with the enzymatic activity, and (2) the atomic structure of human RTCB has not yet been published and neither has its co-structure with NAD(P)(H) or the structures of the super-complex with NAD(P)H and PYROXD1. These structures would allow us to design mutants that do not bind NAD(P)(H) or PYROXD1, providing a tool to test their effects on the regulation of the tRNA-LC. We thus envision that the future structural work would provide new insights into the regulation of the tRNA-LC mechanistically and in the setting of a cell or an organism.

STAR★METHODS

Detailed methods are provided in the online version of this paper and include the following:

SUPPLEMENTAL INFORMATION

Supplemental information can be found online at https://doi.org/10.1016/j.molcel.2021.04.007.

ACKNOWLEDGMENTS

We thank Dhaarsini Koneswarakantha for help and advice, Johannes Popow for experimental suggestions, Sandra Cooper for fruitful discussions, and Life Science Editors for counseling in the writing of the manuscript. We also thank Andrzej Bylicki and Juliane Kley for advice and assistance in the initial crystallization trials, Karin Koch for advice and assistance in the initial pre-steady-state measurements, and Paola Hentges Pinto for assistance in the initial cloning of PYROXD1 for the overexpression in human cells. We want to express gratitude to Michael Riedelberger for advice on metal-ion related experiments. Furthermore, we thank Jutta Dammann, Daniela Zwolanek, Fabian Ackle, and Alessia Duerst for assistance in the purification of recombinant proteins. We also thank staff of beamlines at ESRF (Grenoble) for help during data collection. Work at the Martinez lab was funded by the Medical University of Vienna, the "Fonds zur Förderung der wissenschaftlichen Forschung (FWF)" as Stand-Alone Projects (P29888 and P32011) and through the RNA Biology Doctoral Program. I.A. and A.K. are funded by the Boehringer Ingelheim Fonds PhD Fellowship. Numerical simulations were run on the PARADOX-IV supercomputing facility at the Scientific Computing Laboratory, National Center of Excellence for the Study of Complex Systems, Institute of Physics Belgrade, supported in part by the Ministry of Education, Science and Technological Development of the Republic of Serbia. N.D. and K.N. acknowledge Ministry of Science and Technological Development of the Republic of Serbia contract no.451-03-68/2020-14/200161.

AUTHOR CONTRIBUTIONS

I.A. designed and carried out most of the experiments. E.S. provided guidance for and contributed to carrying out the experiments in anaerobic conditions and pre-steady-state measurements. A.K. designed and carried out the purification of the recombinant tRNA ligase complex, recombinant RTCB, and recombinant Archease, and performed the *in vitro* pull-down experiment. D.P. contributed to carrying out the steady-state measurements and designed and carried out a subset of oligomerization experiments. A.M. collected X-ray diffraction data and determined the X-ray structure of PYROXD1. P.T.-P. generated the inducible *Pyroxd1* KO mouse line and designed and carried out survival experiments. N.D. designed and carried out numerical simulations for the modeling of PYROXD1-cofactor complexes. D.A. designed and carried out the mass spectrometry analysis of the immunoprecipitates. T.S. designed and carried out the transthoracic echocardiography and the histological analysis by trichrome staining. M.J.S. provided guidance for the crystallization experiments and carried out the crystal dehydration. S.S. contributed to the purification of the oligomeric states of PYROXD1 and the subset of steady-state measurements. T.K. designed and carried out the mass spectrometry analysis of FAD. R.B. designed and carried out the native mass spectrometry analysis of PYROXD1. A.S. designed and carried out the co-evolutionary analysis of the tRNA ligase complex members. K.N., M.J., M.H., T.C., J.P., and P.M. provided guidance and contributed to the experimental design and writing of the manuscript. S.W. designed and carried out the experiments. J.M. designed the experiments. I.A., S.W., and J.M. wrote the manuscript.

DECLARATION OF INTERESTS

The authors declare no competing interests.

Received: November 4, 2020
Revised: February 9, 2021
Accepted: April 9, 2021
Published: April 29, 2021

SUPPORTING CITATIONS

The following references appear in the Supplemental information: Antunes et al. (2015); Beveridge et al. (2014); Boehr et al. (2009); Guindon et al. (2010); van Berkel et al. (1999)

REFERENCES

Acosta-Alvear, D., Karagöz, G.E., Fröhlich, F., Li, H., Walther, T.C., and Walter, P. (2018). The unfolded protein response and endoplasmic reticulum protein targeting machineries converge on the stress sensor IRE1. eLife *7*, e43036.

Altschul, S.F., Madden, T.L., Schäffer, A.A., Zhang, J., Zhang, Z., Miller, W., and Lipman, D.J. (1997). Gapped BLAST and PSI-BLAST: a new generation of protein database search programs. Nucleic Acids Res. *25*, 3389–3402.

Antunes, D.A., Devaurs, D., and Kavraki, L.E. (2015). Understanding the challenges of protein flexibility in drug design. Expert Opin. Drug Discov. *10*, 1301–1313.

Argyrou, A., and Blanchard, J.S. (2004). Flavoprotein disulfide reductases: advances in chemistry and function. Prog. Nucleic Acid Res. Mol. Biol. *78*, 89–142.

Banerjee, A., Goldgur, Y., and Shuman, S. (2021). Structure of 3′-PO4/5′-OH RNA ligase RtcB in complex with a 5′-OH oligonucleotide. RNA. https://doi.org/10.1261/rna.078692.121.

Basciu, A., Malloci, G., Pietrucci, F., Bonvin, A.M.J.J., and Vargiu, A.V. (2019). Holo-like and Druggable Protein Conformations from Enhanced Sampling of Binding Pocket Volume and Shape. J. Chem. Inf. Model. *59*, 1515–1528.

Beveridge, R., Covill, S., Pacholarz, K.J., Kalapothakis, J.M., MacPhee, C.E., and Barran, P.E. (2014). A mass-spectrometry-based framework to define the extent of disorder in proteins. Anal. Chem. *86*, 10979–10991.

Bienert, S., Waterhouse, A., de Beer, T.A., Tauriello, G., Studer, G., Bordoli, L., and Schwede, T. (2017). The SWISS-MODEL Repository-new features and functionality. Nucleic Acids Res. *45* (D1), D313–D319.

Boehr, D.D., Nussinov, R., and Wright, P.E. (2009). The role of dynamic conformational ensembles in biomolecular recognition. Nat. Chem. Biol. *5*, 789–796.

Bohnert, K.R., McMillan, J.D., and Kumar, A. (2018). Emerging roles of ER stress and unfolded protein response pathways in skeletal muscle health and disease. J. Cell. Physiol. *233*, 67–78.

Bussi, G., and Laio, A. (2020). Using metadynamics to explore complex free-energy landscapes. Nat. Rev. Phys. *2*, 200–212.

Case, D.A., Ben-Shalom, I.Y., Brozell, S.R., Cerutti, D.S., Cheatham, T.E., Cruzeiro, V.W.D., Darden, T.A., Duke, R.E., Ghoreishi, D., Gilson, M.K., et al. (2018). AMBER 2018 Reference Manual (University of California, San Francisco).

Crooks, G.E., Hon, G., Chandonia, J.M., and Brenner, S.E. (2004). WebLogo: a sequence logo generator. Genome Res. *14*, 1188–1190.

de Hoon, M.J., Imoto, S., Nolan, J., and Miyano, S. (2004). Open source clustering software. Bioinformatics *20*, 1453–1454.

Desai, K.K., Bingman, C.A., Phillips, G.N., Jr., and Raines, R.T. (2013). Structures of the noncanonical RNA ligase RtcB reveal the mechanism of histidine guanylylation. Biochemistry *52*, 2518–2525.

Dolinsky, T.J., Czodrowski, P., Li, H., Nielsen, J.E., Jensen, J.H., Klebe, G., and Baker, N.A. (2007). PDB2PQR: expanding and upgrading automated preparation of biomolecular structures for molecular simulations. Nucleic Acids Res. *35*, W522–W525.

Dolinsky, T.J., Nielsen, J.E., McCammon, J.A., and Baker, N.A. (2004). PDB2PQR: an automated pipeline for the setup of Poisson-Boltzmann electrostatics calculations. Nucleic Acids Res *32*, W665–W667.

Dow, L.E., Premsrirut, P.K., Zuber, J., Fellmann, C., McJunkin, K., Miething, C., Park, Y., Dickins, R.A., Hannon, G.J., and Lowe, S.W. (2012). A pipeline for the generation of shRNA transgenic mice. Nat. Protoc. *7*, 374–393.

El-Gebali, S., Mistry, J., Bateman, A., Eddy, S.R., Luciani, A., Potter, S.C., Qureshi, M., Richardson, L.J., Salazar, G.A., Smart, A., et al. (2019). The Pfam protein families database in 2019. Nucleic Acids Res. *47* (D1), D427–D432.

Emsley, P., and Cowtan, K. (2004). Coot: model-building tools for molecular graphics. Acta Crystallogr. D Biol. Crystallogr. *60*, 2126–2132.

Englert, M., Xia, S., Okada, C., Nakamura, A., Tanavde, V., Yao, M., Eom, S.H., Konigsberg, W.H., Söll, D., and Wang, J. (2012). Structural and mechanistic

insights into guanylylation of RNA-splicing ligase RtcB joining RNA between 3′-terminal phosphate and 5′-OH. Proc. Natl. Acad. Sci. USA *109*, 15235–15240.

Evans, D.J., and Holian, B.L. (1985). The Nose–Hoover thermostat. J. Chem. Phys. *83*, 4069.

Fellmann, C., Hoffmann, T., Sridhar, V., Hopfgartner, B., Muhar, M., Roth, M., Lai, D.Y., Barbosa, I.A., Kwon, J.S., Guan, Y., et al. (2013). An optimized microRNA backbone for effective single-copy RNAi. Cell Rep. *5*, 1704–1713.

Ferreira, P., Villanueva, R., Martínez-Júlvez, M., Herguedas, B., Marcuello, C., Fernandez-Silva, P., Cabon, L., Hermoso, J.A., Lostao, A., Susin, S.A., and Medina, M. (2014). Structural insights into the coenzyme mediated monomer-dimer transition of the pro-apoptotic apoptosis inducing factor. Biochemistry *53*, 4204–4215.

Fiser, A., Do, R.K., and Sali, A. (2000). Modeling of loops in protein structures. Protein Sci. *9*, 1753–1773.

Frisch, M.J., Trucks, G.W., Schlegel, H.B., Scuseria, G.E., Robb, M.A., Cheeseman, J.R., Scalmani, G., Barone, V., Mennucci, B., Petersson, G.A., et al. (2009). Gaussian 09 (Gaussian Inc).

Gogakos, T., Brown, M., Garzia, A., Meyer, C., Hafner, M., and Tuschl, T. (2017). Characterizing Expression and Processing of Precursor and Mature Human tRNAs by Hydro-tRNAseq and PAR-CLIP. Cell Rep. *20*, 1463–1475.

Gradia, S.D., Ishida, J.P., Tsai, M.S., Jeans, C., Tainer, J.A., and Fuss, J.O. (2017). MacroBac: New Technologies for Robust and Efficient Large-Scale Production of Recombinant Multiprotein Complexes. Methods Enzymol. *592*, 1–26.

Greer, C.L., Peebles, C.L., Gegenheimer, P., and Abelson, J. (1983). Mechanism of action of a yeast RNA ligase in tRNA splicing. Cell *32*, 537–546.

Guex, N., Peitsch, M.C., and Schwede, T. (2009). Automated comparative protein structure modeling with SWISS-MODEL and Swiss-PdbViewer: a historical perspective. Electrophoresis *30* (*Suppl 1*), S162–S173.

Guindon, S., Dufayard, J.F., Lefort, V., Anisimova, M., Hordijk, W., and Gascuel, O. (2010). New algorithms and methods to estimate maximum-likelihood phylogenies: assessing the performance of PhyML 3.0. Syst. Biol. *59*, 307–321.

Hanada, T., Weitzer, S., Mair, B., Bernreuther, C., Wainger, B.J., Ichida, J., Hanada, R., Orthofer, M., Cronin, S.J., Komnenovic, V., et al. (2013). CLP1 links tRNA metabolism to progressive motor-neuron loss. Nature *495*, 474–480.

Hentze, M.W., and Preiss, T. (2010). The REM phase of gene regulation. Trends Biochem. Sci. *35*, 423–426.

Hetz, C. (2012). The unfolded protein response: controlling cell fate decisions under ER stress and beyond. Nat. Rev. Mol. Cell Biol. *13*, 89–102.

Hoang, D.T., Chernomor, O., von Haeseler, A., Minh, B.Q., and Vinh, L.S. (2018). UFBoot2: Improving the Ultrafast Bootstrap Approximation. Mol. Biol. Evol. *35*, 518–522.

Holm, L. (2020). DALI and the persistence of protein shape. Protein Sci. *29*, 128–140.

Imlay, J.A., Sethu, R., and Rohaun, S.K. (2019). Evolutionary adaptations that enable enzymes to tolerate oxidative stress. Free Radic. Biol. Med. *140*, 4–13.

Jones, G., Willett, P., Glen, R.C., Leach, A.R., and Taylor, R. (1997). Development and validation of a genetic algorithm for flexible docking. J. Mol. Biol. *267*, 727–748.

Jurkin, J., Henkel, T., Nielsen, A.F., Minnich, M., Popow, J., Kaufmann, T., Heindl, K., Hoffmann, T., Busslinger, M., and Martinez, J. (2014). The mammalian tRNA ligase complex mediates splicing of XBP1 mRNA and controls antibody secretion in plasma cells. EMBO J. *33*, 2922–2936.

Kabsch, W. (2010). Xds. Acta Crystallogr. D Biol. Crystallogr. *66*, 125–132.

Korb, O., Stützle, T., and Exner, T.E. (2009). Empirical scoring functions for advanced protein-ligand docking with PLANTS. J. Chem. Inf. Model. *49*, 84–96.

Kosmaczewski, S.G., Edwards, T.J., Han, S.M., Eckwahl, M.J., Meyer, B.I., Peach, S., Hesselberth, J.R., Wolin, S.L., and Hammarlund, M. (2014). The RtcB RNA ligase is an essential component of the metazoan unfolded protein response. EMBO Rep. *15*, 1278–1285.

Liebschner, D., Afonine, P.V., Baker, M.L., Bunkóczi, G., Chen, V.B., Croll, T.I., Hintze, B., Hung, L.W., Jain, S., McCoy, A.J., et al. (2019). Macromolecular structure determination using X-rays, neutrons and electrons: recent developments in Phenix. Acta Crystallogr. D Struct. Biol. *75*, 861–877.

Lin, J.H., Li, H., Yasumura, D., Cohen, H.R., Zhang, C., Panning, B., Shokat, K.M., Lavail, M.M., and Walter, P. (2007). IRE1 signaling affects cell fate during the unfolded protein response. Science *318*, 944–949.

Lornage, X., Schartner, V., Balbueno, I., Biancalana, V., Willis, T., Echaniz-Laguna, A., Scheidecker, S., Quinlivan, R., Fardeau, M., Malfatti, E., et al. (2019). Clinical, histological, and genetic characterization of PYROXD1-related myopathy. Acta Neuropathol. Commun. *7*, 138.

Lu, Y., Liang, F.X., and Wang, X. (2014). A synthetic biology approach identifies the mammalian UPR RNA ligase RtcB. Mol. Cell *55*, 758–770.

Macheroux, P. (1999). UV-visible spectroscopy as a tool to study flavoproteins. Methods Mol. Biol. *131*, 1–7.

Madeira, F., Park, Y.M., Lee, J., Buso, N., Gur, T., Madhusoodanan, N., Basutkar, P., Tivey, A.R.N., Potter, S.C., Finn, R.D., and Lopez, R. (2019). The EMBL-EBI search and sequence analysis tools APIs in 2019. Nucleic Acids Res. *47* (W1), W636–W641.

Maier, J.A., Martinez, C., Kasavajhala, K., Wickstrom, L., Hauser, K.E., and Simmerling, C. (2015). ff14SB: Improving the Accuracy of Protein Side Chain and Backbone Parameters from ff99SB. J. Chem. Theory Comput. *11*, 3696–3713.

Mair, A., Pedrotti, L., Wurzinger, B., Anrather, D., Simeunovic, A., Weiste, C., Valerio, C., Dietrich, K., Kirchler, T., Nägele, T., et al. (2015). SnRK1-triggered switch of bZIP63 dimerization mediates the low-energy response in plants. eLife *4*, e05828.

McCoy, A.J., Grosse-Kunstleve, R.W., Adams, P.D., Winn, M.D., Storoni, L.C., and Read, R.J. (2007). Phaser crystallographic software. J. Appl. Cryst. *40*, 658–674.

Nguyen, L.T., Schmidt, H.A., von Haeseler, A., and Minh, B.Q. (2015). IQ-TREE: a fast and effective stochastic algorithm for estimating maximum-likelihood phylogenies. Mol. Biol. Evol. *32*, 268–274.

O'Grady, G.L., Best, H.A., Sztal, T.E., Schartner, V., Sanjuan-Vazquez, M., Donkervoort, S., Abath Neto, O., Sutton, R.B., Ilkovski, B., Romero, N.B., et al. (2016). Variants in the Oxidoreductase PYROXD1 Cause Early-Onset Myopathy with Internalized Nuclei and Myofibrillar Disorganization. Am. J. Hum. Genet. *99*, 1086–1105.

Olsson, M.H., Søndergaard, C.R., Rostkowski, M., and Jensen, J.H. (2011). PROPKA3: Consistent Treatment of Internal and Surface Residues in Empirical pKa Predictions. J. Chem. Theory Comput. *7*, 525–537.

Parinello, M. (1981). Polymorphic transitions in single crystals: a new molecular dynamics method. J. Appl. Phys. *52*, 7182.

Peebles, C.L., Ogden, R.C., Knapp, G., and Abelson, J. (1979). Splicing of yeast tRNA precursors: a two-stage reaction. Cell *18*, 27–35.

Perez-Riverol, Y., Csordas, A., Bai, J., Bernal-Llinares, M., Hewapathirana, S., Kundu, D.J., Inuganti, A., Griss, J., Mayer, G., Eisenacher, M., et al. (2019). The PRIDE database and related tools and resources in 2019: improving support for quantification data. Nucleic Acids Res. *47* (D1), D442–D450.

Phizicky, E.M., and Hopper, A.K. (2015). tRNA processing, modification, and subcellular dynamics: past, present, and future. RNA *21*, 483–485.

Popow, J., Englert, M., Weitzer, S., Schleiffer, A., Mierzwa, B., Mechtler, K., Trowitzsch, S., Will, C.L., Lührmann, R., Söll, D., and Martinez, J. (2011). HSPC117 is the essential subunit of a human tRNA splicing ligase complex. Science *331*, 760–764.

Popow, J., Jurkin, J., Schleiffer, A., and Martinez, J. (2014). Analysis of orthologous groups reveals archease and DDX1 as tRNA splicing factors. Nature *511*, 104–107.

Pronk, S., Páll, S., Schulz, R., Larsson, P., Bjelkmar, P., Apostolov, R., Shirts, M.R., Smith, J.C., Kasson, P.M., van der Spoel, D., et al. (2013). GROMACS

4.5: a high-throughput and highly parallel open source molecular simulation toolkit. Bioinformatics *29*, 845–854.

R Development Core Team (2019). R: A language and environment for statistical computing (R Foundation for Statistical Computing).

Ritchie, M.E., Phipson, B., Wu, D., Hu, Y., Law, C.W., Shi, W., and Smyth, G.K. (2015). limma powers differential expression analyses for RNA-sequencing and microarray studies. Nucleic Acids Res. *43*, e47.

Rodríguez, C.I., Buchholz, F., Galloway, J., Sequerra, R., Kasper, J., Ayala, R., Stewart, A.F., and Dymecki, S.M. (2000). High-efficiency deleter mice show that FLPe is an alternative to Cre-loxP. Nat. Genet. *25*, 139–140.

Rowley, D.A., and Halliwell, B. (1985). Formation of hydroxyl radicals from NADH and NADPH in the presence of copper salts. J. Inorg. Biochem. *23*, 103–108.

Sainio, M.T., Välipakka, S., Rinaldi, B., Lapatto, H., Paetau, A., Ojanen, S., Brilhante, V., Jokela, M., Huovinen, S., Auranen, M., et al. (2019). Recessive PYROXD1 mutations cause adult-onset limb-girdle-type muscular dystrophy. J. Neurol. *266*, 353–360.

Schmidt, C.A., and Matera, A.G. (2020). tRNA introns: presence, processing, and purpose. Wiley Interdiscip. Rev. RNA *11*, e1583.

Seo, Y.H., and Carroll, K.S. (2009). Profiling protein thiol oxidation in tumor cells using sulfenic acid-specific antibodies. Proc. Natl. Acad. Sci. USA *106*, 16163–16168.

Spector, D.L., Goldman, R.D., Leinwand, L.A., Harlow, E., and Lane, D. (2005). Immunoblot affinity purification. Nat. Methods *2*, 797–798.

Tribello, G.A., Bonomi, M., Branduardi, D., Camilloni, C., and Bussi, G. (2014). PLUMED 2: new feathers for an old bird. Comput. Phys. Commun. *185*, 604–613.

van Berkel, W.J., Benen, J.A., Eppink, M.H., and Fraaije, M.W. (1999). Flavoprotein kinetics. Methods Mol. Biol. *131*, 61–85.

Vassetti, D., Pagliai, M., and Procacci, P. (2019). Assessment of GAFF2 and OPLS-AA General Force Fields in Combination with the Water Models TIP3P, SPCE, and OPC3 for the Solvation Free Energy of Druglike Organic Molecules. J. Chem. Theory Comput. *15*, 1983–1995.

Walter, P., and Ron, D. (2011). The unfolded protein response: from stress pathway to homeostatic regulation. Science *334*, 1081–1086.

Waterhouse, A., Bertoni, M., Bienert, S., Studer, G., Tauriello, G., Gumienny, R., Heer, F.T., de Beer, T.A.P., Rempfer, C., Bordoli, L., et al. (2018). SWISS-MODEL: homology modelling of protein structures and complexes. Nucleic Acids Res. *46* (W1), W296–W303.

Will, C.L., and Lührmann, R. (2011). Spliceosome structure and function. Cold Spring Harb. Perspect. Biol. *3*, a003707.

Williams, C.J., Headd, J.J., Moriarty, N.W., Prisant, M.G., Videau, L.L., Deis, L.N., Verma, V., Keedy, D.A., Hintze, B.J., Chen, V.B., et al. (2018). MolProbity: more and better reference data for improved all-atom structure validation. Protein Sci. *27*, 293–315.

Wu, C.Y., Hwa, Y.H., Chen, Y.C., and Lim, C. (2012). Hidden relationship between conserved residues and locally conserved phosphate-binding structures in NAD(P)-binding proteins. J. Phys. Chem. B *116*, 5644–5652.

Xiao, W., Wang, R.S., Handy, D.E., and Loscalzo, J. (2018). NAD(H) and NADP(H) Redox Couples and Cellular Energy Metabolism. Antioxid. Redox Signal. *28*, 251–272.

Yoshida, H., Matsui, T., Yamamoto, A., Okada, T., and Mori, K. (2001). XBP1 mRNA is induced by ATF6 and spliced by IRE1 in response to ER stress to produce a highly active transcription factor. Cell *107*, 881–891.

Zuber, J., McJunkin, K., Fellmann, C., Dow, L.E., Taylor, M.J., Hannon, G.J., and Lowe, S.W. (2011). Toolkit for evaluating genes required for proliferation and survival using tetracycline-regulated RNAi. Nat. Biotechnol. *29*, 79–83.

Please cite this article in press as: Asanović et al., The oxidoreductase PYROXD1 uses NAD(P)$^+$ as an antioxidant to sustain tRNA ligase activity in pre-tRNA splicing and unfolded protein response, Molecular Cell (2021), https://doi.org/10.1016/j.molcel.2021.04.007

STAR★METHODS

KEY RESOURCES TABLE

REAGENT or RESOURCE	SOURCE	IDENTIFIER
Antibodies		
anti-beta-actin	Abcam	Cat# ab8226; RRID: AB_306371
anti-RTCB	Bethyl Laboratories	Cat# A305-079A-T; RRID: AB_2631474
anti-DDX1	Bethyl Laboratories	Cat# A300-521A; RRID: AB_451046
anti-CGI-99	Sigma Aldrich	Cat# HPA039824; RRID: AB_10793922
anti-FAM98B	Sigma Aldrich	Cat# HPA008320; RRID: AB_1848419
anti-cysteine Sulfenic Acid (2-Thiodimedone)	Kerafast	Cat# EST022
Bacterial and virus strains		
E. coli BL21(DE3)	IMP Molecular Biology Service	N/A
E. coli BL21 (DE3) Rosetta2	IMP Molecular Biology Service	N/A
E. coli BL834 - Novagen	Merck	Cat# 69041
baculovirus	Generated *in situ*, this paper	N/A
Biological samples		
mouse hearts (see "experimental models")	This paper	N/A
Chemicals, peptides, and recombinant proteins		
Dulbecco's modified Eagle's medium (DMEM)	GIBCO	Cat# 41966-029
fetal bovine serum (FBS)	GIBCO	Cat# A31608-01
penicillin and streptomycin sulfate	Lonza	Cat# 17-602F
hydrogen peroxide (H_2O_2)	Sigma Aldrich	Cat# 1072091000
menadione	Sigma Aldrich	Cat# M5625-25G
thapsigargin	Sigma Aldrich	Cat# T9033
cycloheximide	Sigma Aldrich	Cat# M5625-25G
N-acetylcysteine (NAC)	Sigma Aldrich	Cat# A9165-100G
glycerol	Sigma Aldrich	Cat# G7757-1L
Nonidet P-40 substitute (NP40 substitute)	Fluka	Cat# 74385
4-(2-aminoethyl)benzenesulfonyl fluoride hydrochloride (AEBSF)	AppliChem	Cat# A1421,0100
Dithiothreitol (DTT)	Roche	Cat# 15326321
puromycin	Sigma Aldrich	Cat# P8833-25MG
G418	GIBCO	Cat# 10131035
doxycycline	Sigma Aldrich	Cat# D9891-1G
[α-^{32}P]guanosine-5′-triphosphate	Hartmann Analytic	Cat# SCP-802
spermidine	Sigma Aldrich	Cat# S4139
RNasin	Promega	Cat# N251B
proteinase K	AppliChem	Cat# A3830,0100
cytidine-3′,5′-bisphosphate	PerkinElmer	Cat# NEG019A
T4 RNA ligase 1	NEB	Cat# M0437M
dimethyl sulphoxide (DMSO)	Sigma Aldrich	Cat# D2438-10ML
adenosine triphosphate (ATP)	Thermo Scientific	Cat# R0441

(*Continued on next page*)

Please cite this article in press as: Asanović et al., The oxidoreductase PYROXD1 uses NAD(P)+ as an antioxidant to sustain tRNA ligase activity in pre-tRNA splicing and unfolded protein response, Molecular Cell (2021), https://doi.org/10.1016/j.molcel.2021.04.007

Continued

REAGENT or RESOURCE	SOURCE	IDENTIFIER
guanosine triphosphate (GTP)	Thermo Scientific	Cat# R0461
beta-mercaptoethanol	Merck	Cat# 805740
bovine serum albumin (BSA)	VWR	Cat# 422351S
SequaGel System Buffer	National Diagnostics	Cat# EC-835
SequaGel System Diluent	National Diagnostics	Cat# EC-840
SequaGel System Concentrate	National Diagnostics	Cat# EC-830
formamide	Fluka	Cat# 47670
bromophenol blue	Merck	Cat# 1.08122.0005
Xylene Cyanol	Sigma Aldrich	Cat# X4126-10G
Clarity Western ECL Substrate	Bio-Rad	Cat# 170-5061
TRIzol Reagent	Ambion	Cat# 15596018
salmon sperm DNA	Agilent Technologies	Cat# 201190
ketamine	N/A	N/A
xylazine	N/A	N/A
isoflurane	N/A	N/A
2xTY medium	Carl Roth	Cat# 6676.3
isopropyl-β-D-thiogalactosidase (IPTG)	Fermentas	Cat# R0392
tween-20	Sigma Aldrich	Cat# P1379-1L
chicken egg white lysozyme	Sigma Aldrich	Cat# L6876-10G
cOmplete Protease Inhibitor	Roche	Cat# 11836145001
cOmplete Protease Inhibitor, EDTA free	Roche	Cat# 05056489001
glutathione Sepharose 4B	GE Healthcare	Cat# 17-0756-05
HiLoad Superdex 75 16/60	GE Healthcare	Cat# GE28-9893-33
Amicon Ultra centrifugal filter, MWCO 30 kDa	Merck	Cat# UFC903024
Vivaspin 500 membrane: 30000 MWCO	Sartorius	Cat# VS0122
flavin adenine dinucleotide (FAD)	Sigma Aldrich	Cat# F6625-100MG
selenomethionine	Merck	Cat# 1611955-100MG
sodium-citrate dihydrate	Sigma Aldrich	Cat# W302600
potassium-hydrogen phosphate	Merck	Cat# 1.05104.1000
ammonium-sulfate	AppliChem	Cat# A1032,1000
acetonitrile	N/A	N/A
nicotinamide adenine dinucleotide phosphate, reduced (NADPH)	Roche	Cat# 10107824001
nicotinamide adenine dinucleotide, reduced (NADH)	Sigma Aldrich	Cat# N8129-50MG
nicotinamide adenine dinucleotide phosphate (NADP)	Roche	Cat# 10128031001
nicotinamide adenine dinucleotide (NAD)	Sigma Aldrich	Cat# N0632-5G
ubiquinone-1 (Q1)	Sigma Aldrich	Cat# C7956-10MG
benzyl viologen	Sigma Aldrich	Cat# 271845-250MG
5-deazaFMN	In-house synthesis (Peter Macheroux, TU Graz)	N/A
L-glutathione oxidized (GSSG)	Sigma Aldrich	Cat# G4626-100MG
(L)-dehydroascorbic acid	Sigma Aldrich	Cat# 261556-250MG
L-cystine	Sigma Aldrich	Cat# C8755-100G
(±)-α-Lipoic acid	Sigma Aldrich	Cat# T5625-500MG
insulin, human recombinant	Sigma Aldrich	Cat# I5500-50MG
(+)-sodium L-ascorbate	Sigma Aldrich	Cat# A7631-25G
ascorbate oxidase from *Cucurbita sp*	Sigma Aldrich	Cat# A0157-100UN
polyethylene glycol 400 (PEG 400)	Sigma Aldrich	Cat# 8074851000
2-(N-morpholino)ethanesulphonate hydrate (MES)	AppliChem	Cat# A4730,0250

(*Continued on next page*)

Please cite this article in press as: Asanović et al., The oxidoreductase PYROXD1 uses NAD(P)+ as an antioxidant to sustain tRNA ligase activity in pre-tRNA splicing and unfolded protein response, Molecular Cell (2021), https://doi.org/10.1016/j.molcel.2021.04.007

Continued

REAGENT or RESOURCE	SOURCE	IDENTIFIER
lithium-acetate	Sigma Aldrich	Cat# L4158-100G
tris(2-carboxyethyl)phosphine hydrochloride (TCEP)	Thermo Scientific	Cat# 20491
catalase from bovine liver	Sigma Aldrich	Cat# C30-100MG
Protogel Acrylamide/Bis-acrylamide	National Diagnostics	Cat# EC-890
tris(hydroxymethyl)aminomethane, base (tris)	Fisher Scientific	Cat# BP152-1
glycine	AppliChem	Cat# A1067,5000
HiLoad Superdex 200 16/600	GE Healthcare	Cat# GE28-9893-35
anti-FLAG M2 Affinity Gel	Sigma Aldrich	Cat# A2220-5ML
InstantBlue	Abcam	Cat# ab119211
ammonium-bicarbonate	Sigma Aldrich	Cat# 09830
iodoacetamide	Sigma Aldrich	Cat# I6125
Strep-Tactin	IBA	Cat# 2-1201-010
desthiobiotin	Merck	Cat# D1411
4-(2-hydroxyethyl)-1-piperazineethanesulphonate (HEPES)	Lonza	Cat# BE17-737E
MagStrep type 3 XT beads	IBA	Cat# 2-4090-002
4-15% Mini-PROTEAN® TGX Precast Gel	Bio-Rad	Cat# 4561083
Ni-NTA Superflow resin	QUIAGEN	Cat# 30410
imidazole	Merck	Cat# 56750
His6-tagged Tobacco Etch Virus (TEV) protease	In-house production	N/A
Prescission Protease	IMP Molecular Biology Service	N/A
bathocuproinedisulfonic acid (BCS)	Sigma Aldrich	Cat# B1125-500MG
Chelex 100	Sigma Aldrich	Cat# C7901-25G
copper(II)-sulfate pentahydrate	Fluka	Cat# 61240
iron(II)-chloride	Sigma Aldrich	Cat# 372870-25G
iron(III)-sulfate monohydrate	Sigma Aldrich	Cat# 307718-500G
zinc-chloride	Sigma Aldrich	Cat# 208086-5G
manganese(II)-sulfate monohydrate	Fluka	Cat# 63554
deionized water	In-house production	N/A
dimedone	Sigma Aldrich	Cat# D153303
Dynabeads M-280 Streptavidin	Thermo Scientific	Cat# 11205D
biotinylated-NAD	Trevigen	Cat# 4670-500-01
Critical commercial assays		
T7 MEGAshortscript kit	Thermo Scientific	Cat# AM1354
Masson Trichrome with aniline blue	Bio Optica	Cat# 04-010802A
GoTaq® qPCR Master Mix	Promega	Cat# A6002
Maxima First Strand cDNA Synthesis Kit	Thermo Scientific	Cat# K1672
CalPhos Mammalian Transfection Kit	Takara Bio	Cat# 631312
Bac-to-Bac Baculovirus expression system	Thermo Fischer	Cat# 10359016
Trans-Blot Turbo RTA Transfer Kit, PVDF	Bio-Rad	Cat# 1704273
Deposited data		
structural model of PYROXD1	PDB	6ZK7
mass spectrometry data	PRIDE	PXD018831
Experimental models: cell lines		
HeLa (ATCC CCL-2)	Thermo Scientific	N/A
Tet-ON HeLa	This paper	N/A
Flp-In-T-REx-HEK293	Thermo Scientific	N/A
Sf9 Cell Line	gift from Petr Cejka, IRB Bellinzona; ATCC	Cat# ATCC CRL-1711

(*Continued on next page*)

Please cite this article in press as: Asanović et al., The oxidoreductase PYROXD1 uses NAD(P)$^+$ as an antioxidant to sustain tRNA ligase activity in pre-tRNA splicing and unfolded protein response, Molecular Cell (2021), https://doi.org/10.1016/j.molcel.2021.04.007

Continued

REAGENT or RESOURCE	SOURCE	IDENTIFIER
FLAG-PYROXD1 HEK293	This paper	N/A
Experimental models: organisms/strains		
Pyroxd1$^{tm1a(KOMP)Wtsi}$ Knockout First mice	KOMP	Cat# CSD84611
FRTe mouse	Rodríguez et al., 2000	N/A
A1*cf.*$^{Tg(Myh6-cre/Esr1*)1Jmk}$	Jackson Laboratory	Cat# 005657
Oligonucleotides		
primer for shRNA cloning miR-E_fwd: 5′-TAC AAT ACT CGA GAA GGT ATA TTG CTG TTG ACA GTG AGC G-3′	Sigma Aldrich	N/A
primer for shRNA cloning miR-E_rev: 5′-TTA GAT GAA TTC TAG CCC CTT GAA GTC CGA GGC AGT AGG CA-3′	Sigma Aldrich	N/A
primer for yeast pre-tRNA: 5′-AAT TTA ATA CGA CTC ACT ATA GGG GAT TTA GCT CAG TTG GG- 3′	Sigma Aldrich	N/A
primer for yeast pre-tRNA: 5′-TGG TGG GAA TTC TGT GGA TCG AAC-3′	Sigma Aldrich	N/A
RNA oligonucleotide from the firefly luciferase 5′-UCG AAG UAU UCC GCG UAC GU-3′	Dharmacon	N/A
complementary oligonucleotide for annealing: 5′-CGU ACG CGG AAU ACU UCG A-3′	Dharmacon	N/A
tyrosine-tRNA 5′ exon probe, 5′-CT*A CA*G TC*C TC*C GC*T CT*A CC-3′ (* denotes LNA nucleotide)	Exiqon	N/A
tyrosine-tRNA 5′ exon probe, 5′- CTA CAG TCC TCC GCT CTA CCA-3′	Exiqon	N/A
methionine 5′ tRNA probe, 5′-GGG CCC AGC ACG CTT CCG CTG CGC CAC TCT GC-3′	Exiqon	N/A
U6 snRNA probe: 5′-GCA GGG GCC ATG CTA ATC TTC TCT GTA TCG-3′	Exiqon	N/A
PYROXD1 cloning primer: 5′- CGC GGA TCC ATG GAG GCA GCG CGC CCT CC-3′	Sigma Aldrich	N/A
PYROXD1 cloning primer: 5′- TAG CCG CTC GAG TTA GTC AAA ATA ATC TTC TA-3′	Sigma Aldrich	N/A
Recombinant DNA		
RT3GEN Tet-shRNA expression vector	gift of Johannes Zuber, IMP	N/A
pcDNA5/FRT mammalian expression vector	gift of Alfredo Castello, University of Oxford	N/A
pGEX-6P-1 vector	Cytiva	Cat# 28954648
pWPXLd backbone	Addgene	Cat# 12258
miR-E backbone of RT3GEN	gift of Johannes Zuber, IMP	N/A
438-Rgfp	Addgene	Cat# 55221
MacroLab pFastBac vector 438-A	Addgene	Cat# 55218
MacroLab pFastBac vector 438-B	Addgene	Cat# 55219
MacroLab pFastBac vector 438-Rgfp	Addgene	Cat# 55221
MacroLab 4B vector	Addgene	Cat# 30115
MacroLab 2M-T vector	Addgene	Cat# 29708
Software and algorithms		
Protein-Protein BLAST	NCBI	Version 2.2.28+
ClustalW	GenomeNet	N/A
IQTree	CIBIV/UniVie	Version 1
WebLogo	UC Berkeley	N/A
ImageQuant	GE Healthcare	TL 8.1
Fujifilm VisualSonics Preclinical Imaging Platform	Fujifilm	VEVO 770
PRISM	GraphPad	Version 8

(*Continued on next page*)

Please cite this article in press as: Asanović et al., The oxidoreductase PYROXD1 uses NAD(P)$^+$ as an antioxidant to sustain tRNA ligase activity in pre-tRNA splicing and unfolded protein response, Molecular Cell (2021), https://doi.org/10.1016/j.molcel.2021.04.007

Continued

REAGENT or RESOURCE	SOURCE	IDENTIFIER
DALI server	University of Helsinki	N/A
Kinetic Studio software	TgK Scientific Limited	N/A
MaxQuant	Max Plank Institute	N/A
Masslynx	Waters	Version 4.1
PHASER	University of Cambridge	N/A
COOT	MRC Laboratory of Molecular Biology	N/A
MolProbity	Duke University	N/A
LIMMA	Bioconductor	N/A
PyMol	Schrödinger, Inc.	Version 2.0.7
Modeler	BIOVIA	Version 9.21
PROPKA server	Olsson et al., 2011	Version 3.0
PDB2PQR server	(Dolinsky et al., 2004)	Version 2.0.0
GOLD	CCDC	Version 5.6.0
Gaussian09	Frisch et al., 2009	Revision A.02
CHEMPLP	CCDC	N/A
PLUMED	Tribello et al., 2014	Version 2.3.5
GROMACS	Pronk et al., 2013	Version 2016.6
xLeap	AmberTools	N/A
Other		
Phosphoscanner Amersham Typhoon 5	GE healthcare	Model: 29187191
ChemiDoc Touch	Bio-Rad	Model: 1708370
VisualSonics 700-Series RMV Scanhead	Fujifilm	Model: RMV707B
Omni Sonic Ruptor 250	Omni Interactions	N/A
ÄKTA purifier GE	GE Healthcare	N/A
Ultimate 3000 HPLC	Thermo Scientific	N/A
TSQ Vantage mass spectrometer	Thermo Scientific	N/A
Specord 200 plus	Analytik Jena	N/A
glove box	Belle Technology	N/A
10 W LED floodlight	Luminea	N/A
SF-61SX2 stopped flow	TgK Scientific	N/A
PM-61 s photomultiplier	TgK Scientific	N/A
Hybrid Multi-Mode Microplate Reader	Synergy H1	N/A
Mosquito	TTP Biotech	Version 3.10
Synapt G2Si	Waters	N/A
Q Exactive HF-X Orbitrap mass spectrometer	Thermo Scientific	N/A
Ultimate 3000 RSLC nano-flow chromatography system	Thermo Scientific	N/A
DynaMag-5 Magnet holder	Thermo Scientific	N/A

RESOURCE AVAILABILITY

Lead contact

Further information and requests for resources and reagents should be directed to and will be fulfilled by the Lead Contact, Javier Martinez (javier.martinez@meduniwien.ac.at).

Materials availability

Proprietary material is available upon request from the authors.

Data and code availability

Raw data and quantification data are available at Mendely Data: https://data.mendeley.com/datasets/xcf7cdjrpg/draft?a=1dd6130d-d375-4b7f-9055-c96be72e2ebd.

The mass spectrometry proteomics data have been deposited to the ProteomeXchange Consortium via the PRIDE partner repository with the dataset identifier PXD018831. The X-ray diffraction data are deposited in PDB entry Crystal Structure of human PYROXD1/FAD complex, PDB code 6ZK7. Additional intermediary data are available directly from the authors.

EXPERIMENTAL MODEL AND SUBJECT DETAILS

Mouse model

Pyroxd1$^{tm1a(KOMP)Wtsi}$ Knockout First mice were acquired from the KOMP Repository Knockout Mouse Project (https://www.komp.org, catalog #CSD84611) and were bred as heterozygous (C57BL/6N-A^{tm1Brd} strain). Heterozygous *Pyroxd1*$^{tm1a(KOMP)Wtsi}$ mice were crossed with FRTe (Rodríguez et al., 2000) to obtain *Pyroxd1*$^{fl/+}$ mice. The removal of FRT-LacZ-neo-FRT was identified by PCR genotyping (data not shown). *Pyroxd1*$^{fl/+}$ mice were backcrossed on to C57BL/6J genetic background and finally bred as homozygous animals (*Pyroxd1*$^{fl/fl}$).

To generate cardiomyocyte specific *Pyroxd1* knockout mice, A1*cf.*$^{Tg(Myh6-cre/Esr1*)1Jmk}$ (αMHC-MerCreMer, Jackson Laboratory, #005657) mice were bred with *Pyroxd1*$^{fl/fl}$ mice for two generations to obtain *Pyroxd1*$^{fl/fl}$;αMHC-MerCreMer tamoxifen-inducible conditional knockout mice. *Pyroxd1*$^{fl/+}$;αMHC-MerCreMer, *Pyroxd1*$^{+/+}$;αMHC-MerCreMer and *Pyroxd1*$^{fl/+}$ were used as control mice in this study. No αMHC-MerCreMer/αMHC-MerCreMer mice were used. To induce Cre-expression, mice were injected with 10 mg·kg^{-1} tamoxifen once per day for four consecutive days.

Animals were maintained under a 14-hours light/10-hours dark cycle, and provided with food and water *ad libitum*. All animal experiments were performed according to EU-directive 2010/63/EU. The experiments were performed on gender balanced cohorts of adult mice aged between 8 and 10 weeks.

Ethics statement

All animal studies, handling, and sacrificing were approved by the Austrian Federal Ministry of Science and Research (permit no. BMWF—66.015/0020-V/3b/2019) and were undertaken in strict accordance with prevailing guidelines for animal care and welfare.

Cell lines

HeLa (ATCC® CCL-2), Tet-ON HeLa cell lines, and Flp-In™-T-REx™-HEK293 (Thermo Fisher Scientific) were cultured at 37°C, 5% CO_2 in Dulbecco's modified Eagle's medium (GIBCO) supplemented with 10% fetal bovine serum (GIBCO), 100 U·mL^{-1} penicillin, and 100 μg·mL^{-1} streptomycin sulfate (Lonza) and routinely tested for mycoplasma.

To generate ecotropically infectible Tet-ON HeLa cells, we constructed a lentivirus co-expressing the ecotropic receptor (EcoR), rtTA3, and Puro by shuttling the according expression cassette from pRIEP (Zuber et al., 2011) into the pWPXLd backbone (Addgene plasmid 12258). HeLa cells transduced with pWPXLd-EF1-EcoR-IRES-rtTA3-PGK-Puro (pWPXLd-RIEP) were selected with 2 μg·mL^{-1} puromycin (Sigma Aldrich) and subsequently retrovirally transduced with ecotropically packaged RT3GEN Tet-shRNA expression vectors (see section "Cloning of shRNAs") (Zuber et al., 2011). For knockdown, cells were transduced with a single shRNA expression vector and selected with 1 mg·mL^{-1} G418 (GIBCO). Tet-regulated shRNA expression was induced by treatment of these cells for 6 days with 1 μg·mL^{-1} doxycycline (Dox, Sigma) added to the medium. Cell culture medium supplemented with selection antibiotics and Dox was replaced every second day.

To generate FLAG-tagged PYROXD1 cell line, full-length human PYROXD1 open reading frames was PCR-amplified from HeLa cDNA and introduced into a pcDNA5/FRT mammalian expression vector N-terminally encoding for a FLAG-HA tag (kind gift of Alfredo Castello, University of Oxford), designed for the use with the Flp-In™ system (Thermo Fisher Scientific). Flp-In™-T-REx™-HEK293 cells, encoding an FRT integration site and the tet-repressor system, were transfected using CalPhos Mammalian Transfection Kit. Isogenic cell lines carrying integrated genes were selected by Hygromycin B resistance, polyclonally pooled and validated for PYROXD1 gene expression.

Expression systems

PYROXD1 was expressed in bacterial expression system. *Escherichia coli* BL21(DE3) were transformed with the pGEX-6P-1 plasmid encoding for GST-PYROXD1 WT and mutant variants and grown at 37°C, 120 rpm in 2xTY medium in presence of ampicillin (final concentration 0.1 mg·mL^{-1}). At optical density (600 nm) of 0.4, the temperature was dropped to 18°C and at optical density (600 nm) of 1.0, isopropyl-β-D-thiogalactosidase (IPTG, Fermentas, final concentration 0.1 mmol·L^{-1}) was added. After overnight incubation under the same conditions, bacteria were collected by centrifugation at 4°C, 4500 min^{-1} for 10 min.

Archease was expressed using bacterial expression system. DNA encoding human Archease (Uniprot Q8IWT0) spanning residues 27–167 was cloned into the UC Berkeley MacroLab 2M-T vector (gift from Scott Gradia, Addgene plasmid #29708) to express a fusion protein containing an N-terminal His_6 tag, maltose binding protein (MBP) tag, and a TEV-protease cleavage site. The fusion protein was expressed in BL21 (DE3) Rosetta2 *Escherichia coli* cells induced with 0.2 mM IPTG at 18°C overnight.

Recombinant RTCB was expressed using insect cell expression system. DNA encoding the human RTCB (Uniprot Q9Y3I0) was cloned into the UC Berkeley MacroLab 4B vector (gift from Scott Gradia, Addgene plasmid #30115). The fusion protein containing an N-terminal His_6 tag and a TEV-protease cleavage site was expressed in Sf9 insect cells using the Bac-to-Bac Baculovirus expression system (Thermo Scientific). Cells were harvested 60 h after infection.

Recombinant tRNA-LC was expressed using insect cell expression system. DNA sequences encoding the four subunits of the human tRNA ligase complex, RTCB (Uniprot Q9Y3I0), DDX1 (Uniprot Q92499), CGI-99 (Uniprot Q9Y224), and FAM98B (Uniprot Q52LJ0) were inserted using ligation-independent cloning into the UC Berkeley MacroLab pFastBac vectors 438-A, 438-B, 438-A, and 438-Rgfp, respectively. The vectors were gift from Scott Gradia, Addgene plasmids #55218 (438-A), #55219 (438-B), and #55221 (438-Rgfp). The four subunits were combined into a single baculovirus transfer plasmid using the MacroBac protocol (Gradia et al., 2017). The final plasmid encoded untagged RTCB, DDX1 with an N-terminal His_6 tag and TEV-protease cleavage site, untagged CGI-99, and FAM98B with N-terminal StrepII and GFP tags followed by a TEV-protease cleavage site. Recombinant baculoviruses were generated using the Bac-to-Bac Baculovirus expression system (Invitrogen) and the proteins were expressed in Sf9 insect cells infected at a density of 1.0×10^6 ml_{-1}. Cells were harvested 60 h after infection.

METHOD DETAILS

Phylogenetic profiling

We selected 188 species for a wide taxonomic range in Bacteria, Archaea and Eukarya with complete proteomes from various sources, such as NCBI, UniProt, and ENSEMBL (status 02/2014). Orthologous relationships were defined as bidirectional best hits with NCBI Protein-Protein BLAST version 2.2.28+ (Altschul et al., 1997) and restricted to an E-value threshold of 0.1, resulting in a matrix of 21733 human genes with presence or absence in 187 organisms. The table was reduced to 14303 genes by removing phylogenetic patterns that were present or absent in > = 95 percent of all organisms and analyzed by hierarchical gene clustering using cluster 3.0 with Euclidean distance and pairwise average-linkage (de Hoon et al., 2004). The tRNA-LC members CGI-99 and DDX1 were combined in one cluster (distance: 0.88) and the next node was PYROXD1 (distance: 0.81). RTCB and Archease were merged in one cluster as well (distance 0.7), but not related to the CGI-99/DDX1/PYROXD1 cluster.

Phylogenetic tree and sequence logos

To construct a phylogenetic tree, the sequences of 65 proteins included in the seed group for Pyr_redox_2 domain in the Pfam database (status 3/2020) (El-Gebali et al., 2019), together with PYROXD1 and mitochondrial apoptosis-inducing factor-1 (AIFM1) were first used to generate a multiple sequence alignment using ClustalW, with the settings: Gap Open Penalty 10, Gap Extension Penalty 0.5, no weight transition, hydrophilic residues GPSNDQERK, with hydrophilic gaps and BLOSOM as weight matrix (Madeira et al., 2019). The sequence alignment file was then uploaded to the IQTree server to generate the phylogenetic tree, with the following settings: 1000 bootstep alignments, 1000 maximum iterations, 1000 replicates for single branch test, 0.99 minimum correlation coefficient, perturbation strength 0.5 and IQ-Tree stopping rule 100 (Hoang et al., 2018; Nguyen et al., 2015). The same set of sequences was uploaded to WebLogo tool to generate the sequence logo image (Crooks et al., 2004).

Cloning of shRNAs

For RNAi-mediated depletion of PYROXD1, shRNAs were designed using the online siRNA prediction tool: 'Designer of Small Interfering RNAs—DSIR' (http://biodev.extra.cea.fr/DSIR/DSIR.html), also described in Dow et al. (2012). The respective 97-mer oligonucleotides (Integrated DNA technologies) were cloned into the optimized miR-E backbone of RT3GEN (Fellmann et al., 2013). In detail, following top-scoring 21-mer 'Guide strand' output from DSIR was incorporated into a 97-mer PCR template (guide sequences is marked in bold), with the nucleotide 5′ upstream of the 21-mer sense strand being adapted depending on the nucleotide 5′ to the 21-mer target site in the mRNA transcript (Dow et al., 2012):

PYROXD1 shRNA 97-mer: TGCTGTTGACAGTGAGCGACAGCTGAATTCTTGACTTCAATAGTGAAGCCACAGATGTA**TTGAAGT CAAGAATTCAGCTGC**TGCCTACTGCCTCGGA

In addition, a control shRNA template targeting *Renilla* luciferase was used (Zuber et al., 2011):

Control shRNA 97-mer: TGCTGTTGACAGTGAGCGCAGGAATTATAATGCTTATCTATAGTGAAGCCACAGATGTATAGATAAG CATTATAATTCCTATGCCTACTGCCTCGGA

For the PCR reaction, following primers were used (Fellmann et al., 2013): miR-E_fwd-XhoI: 5′-TAC AAT ACT CGA GAA GGT ATA TTG CTG TTG ACA GTG AGC G-3′ and miR-E_rev-EcoRI: 5′-TTA GAT GAA TTC TAG CCC CTT GAA GTC CGA GGC AGT AGG CA-3′. Upon cloning into XhoI and EcoRI restriction sites of RT3GEN, the obtained RT3GEN Tet-shRNA constructs were used for ecotropical packaging and subsequent retroviral transduction of HeLa cells (pWPXLd-RIEP), as described in the section "Cell lines."

Cell culture and cell extract preparation

HeLa (ATCC® CCL-2) cells were cultured as described above (see Experimental model and subject details – Cell lines). Cell treatments were performed including the following reagents to the cell medium at the indicated concentrations and time periods: hydrogen peroxide (Sigma), menadione (Sigma), thapsigargin (Sigma), cycloheximide (Sigma; 10 $\mu g \cdot mL^{-1}$ final concentration), and N-Acetylcysteine (Sigma; 2 mM final concentration). Cell extracts for RNA processing assays and western blot analysis were

Please cite this article in press as: Asanović et al., The oxidoreductase PYROXD1 uses NAD(P)$^+$ as an antioxidant to sustain tRNA ligase activity in pre-tRNA splicing and unfolded protein response, Molecular Cell (2021), https://doi.org/10.1016/j.molcel.2021.04.007

prepared by harvesting cells in lysis buffer (30 mM HEPES pH 7.4, 100 mM KCl, 5 mM $MgCl_2$, 10% (v/v) glycerol, 1% (v/v) Nonidet P-40, 0.1 mM AEBSF, 1 mM DTT). Extracts were cleared by centrifugation, flash frozen in liquid nitrogen and stored at −80°C. For the siRNA mediated-knockdown of RTCB in HeLa cells, an ON-TARGET*plus* siRNA SMARTpool was obtained from Dharmacon. HeLa cells were transfected using the Lipofectamine® RNAiMax (Invitrogen) reagent according to manufacturer's instructions, and silencing was performed for 6 days in total, with an additional siRNA-transfection step after the first 3 days.

tRNA splicing assay

A PCR was performed using *S. cerevisiae* genomic DNA as template, a 5′ primer including the T7 polymerase promoter (5′-AAT TTA ATA CGA CTC ACT ATA GGG GAT TTA GCT CAG TTG GG- 3′), and a 3′ primer (5′-TGG TGG GAA TTC TGT GGA TCG AAC-3′). The PCR product was sequenced and identified as yeast tRNA3-Phe^{GAA} (chromosome 13). The PCR product served as template for *in vitro* transcription using the T7 MEGAshortscript kit (Ambion) including 1.5 MBq [α-^{32}P]guanosine-5′-triphosphate (111 TBq·mmol^{-1}, Hartmann Analytic) per reaction. The pre-tRNA was resolved in a 10% denaturing polyacrylamide gel, visualized by autoradiography and passively eluted from gel slices overnight in 0.3 M NaCl. RNA was precipitated by addition of three volumes of ethanol and dissolved at 0.1 μM in buffer containing 30 mM HEPES-KOH pH 7.3, 2 mM $MgCl_2$, 100 mM KCl. To assess pre-tRNA splicing, one volume of 0.1 μM body-labeled *S. cerevisiae* pre-tRNA^{Phe}, pre-heated at 95°C for 60 s and incubated for 20 min at room temperature, was mixed with four volumes of reaction buffer (100 mM KCl, 5.75 mM $MgCl_2$, 2.5 mM DTT, 5 mM ATP, 6.1 mM Spermidine-HCl pH 8.0 (Sigma), 100 U·mL^{-1} RNasin RNase inhibitor [Promega]). Equal volumes of this reaction mixture and cell extracts (protein concentration 3-6 mg·mL^{-1}) were mixed and incubated at 30°C for 30 minutes. The reaction mix was subsequently deproteinized with proteinase K, followed by phenol/chloroform extraction and ethanol precipitation. Reaction products were separated on a 10% denaturing polyacrylamide gel, and mature tRNA formation and tRNA exon formation was monitored by phosphorimaging.

RNA ligation assays

Substrate preparation

50 pmol RNA oligonucleotide derived from the firefly luciferase gene (5′-UCG AAG UAU UCC GCG UAC GU-3′, Dharmacon) were incubated with 1.11 MBq [5′-32P] cytidine-3′,5′-bisphosphate (111 TBq·mmol^{-1}, Perkin Elmer) and 20 units T4 RNA ligase 1 (NEB) for 1 hr at 16°C in 15% (v/v) DMSO, 50 mM Tris-HCl pH 7.6, 10 mM MgCl2, 10 mM beta-mercaptoethanol, 200 μM ATP, 0.1 mg·mL^{-1} BSA in a total reaction volume of 10 μL. Labeling reactions were resolved by denaturing gel electrophoresis in 15% polyacrylamide gels containing 8 M urea (SequaGel, National Diagnostics). The 3′ end-labeled RNA was visualized by autoradiography and passively eluted from gel slices overnight at 4°C in 0.3 M NaCl. The RNA was precipitated by adding three volumes of ethanol and used directly for intra-strand ligation (circularization) assay using recombinant proteins.

Intra-strand ligation (circularization) assay (for recombinant proteins)

Activity of the recombinant tRNA-LC and RTCB was measured using an RNA (circularization) ligation assay. In short, the solution containing 12.5 mM TCEP, 100 mM KCl, 2.9 mM $MgCl_2$, 7.5 mM ATP, 0.5 mM GTP, 250 μM $ZnCl_2$, RNasin® Ribonuclease Inhibitors (1 μL per 500 μL) and 65% (v/v) glycerol was first mixed (2/1, v/v) with radiolabelled oligoribonucleotide (described above) to prepare the reaction cocktail. The cocktail was then mixed (3/2, v/v) with the sample containing recombinant tRNA-LC or RCTB, and Archease (see "In vitro reconstitution system experiments"), and incubated for 30 min at 30°C. The reaction was then stopped with 2xFA solution (1/1, v/v), composed of 90% Formamide, 50 mM EDTA, 1 ng·mL^{-1} bromophenol blue, 1ng·mL^{-1} Xylene Cyanol and boiled for 1 min. The reaction products were separated on a denaturing 15% urea-polyacrylamide gel (SequaGel) and detected by autoradiography. ImageQuant software was used to quantify the band intensities and substrate conversion rate was calculated as the quotient of the substrate and the sum of substrate and product band intensities. When done in independent replicates, the results are represented as the average value with the standard error of the mean (σ = 0.05).

Inter-strand ligation assay (for cell extracts)

For the use in inter-strand ligation assays using cell extracts, the RNA was annealed to a non-labeled, complementary RNA oligonucleotide (5′-CGU ACG CGG AAU ACU UCG A-3′, Dharmacon, Thermo Scientific). (3/5)th volumes of a reaction mixture (67 mM KCl, 2 mM $MgCl_2$, 8.3 mM DTT, 5 mM ATP, 0.3 mM GTP, 53 U·mL^{-1} RNasin RNase inhibitor, 43% glycerol) containing 17 nM radiolabelled RNA duplex were mixed with 2/5 volumes of cell extracts (protein concentration 3-6 mg·mL^{-1}) and incubated at 30°C for 30 minutes. Reaction products were subsequently separated on a 15% denaturing polyacrylamide gel, and ligation products were monitored by phosphorimaging. Quantification of band intensities was performed using the ImageQuant software.

Western blotting

Protein concentration was determined using Bradford assay and 25 μg of each sample were separated by SDS-PAGE, transferred onto Immuno-Blot® PVDF membranes (Bio-Rad) and probed with antibodies against beta-actin (Abcam), FLAG M2 (Sigma), RTCB (Bethyl Laboratories), DDX1 (Bethyl Laboratories), CGI-99 (Sigma), FAM98B (Sigma), and cysteine Sulphenic Acid (2-Thiodimedone) (Kerafast), using standard protocols. An antibody against PYROXD1 was produced by immunization of rabbits using full-length recombinant human PYROXD1 (LMU Munich, Germany). Subsequently, the antibody was affinity-purified on the recombinant protein, immobilized on nitrocellulose membrane strip (Spector et al., 2005). Western blots were developed using Clarity Western ECL Substrate (Bio-Rad) as recommended by the manufacturer.

Please cite this article in press as: Asanović et al., The oxidoreductase PYROXD1 uses NAD(P)$^+$ as an antioxidant to sustain tRNA ligase activity in pre-tRNA splicing and unfolded protein response, Molecular Cell (2021), https://doi.org/10.1016/j.molcel.2021.04.007

Northern blot analyses

Isolation of total RNA from HeLa cells and mouse tissues was performed using the TRIzol Reagent (Ambion) according to the manufacturer's instructions. Typically, 4-5 μg of RNA was separated in a 10% denaturing polyacrylamide gel (20 × 25 cm; Sequagel, National Diagnostics). The RNA was blotted on Hybond-N+ membranes (GE Healthcare) and fixed by ultraviolet cross-linking. Membranes were pre-hybridized in 5X SSC, 20 mM Na_2HPO_4 pH 7.2, 7 % SDS, and 0.1 mg·mL^{-1} sonicated salmon sperm DNA (Stratagene) for 1 hr at 80°C (for DNA/LNA probes) or 50°C (for DNA probes). Hybridization was performed in the same buffer overnight at 80°C (for DNA/LNA probes) or 50°C (for DNA probes) including 100 pmol of the following [5′-^{32}P]-labeled DNA/LNA probes (Exiqon, Denmark; LNA nucleotides are indicated by "*X"): tyrosine-tRNA 5′ exon probe, 5′-CT*A CA*G TC*C TC*C GC*T CT*A CC-3′; or following DNA probes: tyrosine-tRNA 5′ exon probe, 5′- CTA CAG TCC TCC GCT CTA CCA-3′, methionine 5′ tRNA probe, 5′-GGG CCC AGC ACG CTT CCG CTG CGC CAC TCT GC-3′. Subsequently blots were washed twice for 1 min at 80°C (for DNA/LNA probe) or 50°C (for DNA probe) with 5X SSC, 5% SDS and once for 1 min with 1X SSC, 1% SDS and analyzed by phosphorimaging. Membranes were re-hybridized at 50°C using a DNA probe (5′-GCA GGG GCC ATG CTA ATC TTC TCT GTA TCG-3′) complementary to U6 snRNA to check for equal loading.

Quantitative reverse transcriptase PCR

Total RNA was prepared using TRIzol reagent (Ambion). RNA (1 μg) was DNase treated and reverse-transcribed using the Maxima First Strand cDNA Synthesis Kit for RT-qPCR with dsDNase (Thermo Fisher Scientific) according to the manufacturer's instructions. cDNA was diluted 1:10 prior to analysis by quantitative PCR using the GoTaq® qPCR Master Mix (Promega). The following primers were used (Jurkin et al., 2014): human ACTB: 5′-TTG CCG ACA GGA TGC AGA AGG A-3′ (fwd) and 5′-AGG TGG ACA GCG AGG CCA GGA T-3′ (rev); human XBP1s: 5′-GAG TCC GCA GCA GGT G-3′ (fwd, primer spanning the non-conventional exon–exon junction) and 5′-GGA AGG GCA TTT GAA GAA CA-3′ (rev); human total XBP1: 5′-GCG CTG AGG AGG AAA CTG AAA AAC-3′ (fwd) and 5′-CCA AGC GCT GTC TTA ACT CC-3′ (rev); human XBP1u: 5′-ACT ACG TGC ACC TCT GCA G-3′ (fwd) and 5′-GGA AGG GCA TTT GAA GAA CA-3′ (rev). Following parameters were used for PCR: 50°C for 10 min, 95°C for 5 min, followed by 60 cycles in total at 95°C for 10 s and 60°C for 30 s. The obtained data were analyzed according to the $\Delta\Delta C_t$ method. mRNA expression levels were normalized to *ACTB* and additionally to the indicated control samples. Results were statistically compared using unpaired Student's t test.

Survival curve

To monitor survival, cardiomyocyte specific *Pyroxd1* knockout, and control mice (see Experimental model and subject details – Mouse model) injected with tamoxifen were kept in groups of three to five animals per cage without any other treatment over a minimum of 50 days.

Assessment of cardiac function by transthoracic echocardiography and histological analysis by trichrome staining

Cardiac function was measured with echocardiography at the indicated time points, followed by harvesting of the hearts for further experiments. To cultivate hearts, mice were anesthetized with ketamine 80mg·kg^{-1} and xylazine 5mg·kg^{-1} by intraperitoneal injection and hearts were collected immediately. The hearts used for Northern blot analyses were directly snap frozen in liquid nitrogen and kept at −80°C until further processing. Hearts for histological analysis were incubated in 1x PBS with 30 mM KCl to arrest them in diastole followed by fixation in 4 % PFA at room temperature overnight. After fixation the hearts were embedded in paraffin and subsequently serial sections were acquired using a microtome. Selected sections were stained with Masson's trichrome staining (Masson Trichrome with aniline blue, Bio Optica) according to manufacturer's instructions to analyze fibrosis.

Transthoracic echocardiography was performed using a Fujifilm VisualSonics Preclinical Imaging Platform (VEVO 770) with a RMV707B high-frequency scanhead. Parasternal long axis B-mode and M-mode images were acquired, left ventricular (LV), end-diastolic volume (LVEDV), end-systolic volume (LVESV), end-diastolic diameter (LVEDD), and end-systolic diameter (LVESD) were measured, as well as LV ejection fraction (EF) and LV fractional shortening (FS) calculated using the software provided with the imaging platform. Anaesthesia for imaging was induced with 4 % isoflurane and sustained with 1.5 % isoflurane in oxygen. The investigator performing the measurements was blinded for the genotypes.

Cloning of PYRXOD1 for recombinant protein expression and directed mutagenesis

The full-length coding sequence of human PYROXD1 was amplified from HeLa cDNA by polymerase chain reaction (PCR) using primers BamHI_PYROXD1_F (5′- CGC GGA TCC ATG GAG GCA GCG CGC CCT CC-3′) and XhoI_PYROXD1_R (5′- TAG CCG CTC GAG TTA GTC AAA ATA ATC TTC TA-3′). The amplified sequence was ligated into the pGEX-6P-1 vector (GE Healthcare) upon cleavage with the restriction enzymes BamHI and XhoI.

Expression and purification of recombinant PYROXD1

Upon overnight expression of PYROXD1 (see Experimental model and subject details – Expression systems), bacteria were collected by centrifugation at 4°C, 4500 min^{-1} for 10 min. They were then resuspended in the lysis buffer (100 mL per 1 L of bacterial culture), containing 50 mM Tris HCl pH 8.0, 100 mM NaCl, 5 mM $MgCl_2$, 1 μM AEBSF, 0.1% (v/v) Tween-20, 1 mg·mL^{-1} chicken egg white lysozyme, and one proteinase inhibitor tablet per 100 mL (cOmplete Protease Inhibitor, EDTA free). After 30 min (18 rpm, 4°C) of lysis in the buffer, bacteria were further lysed by sonication (Omni Sonic Ruptor 250), using following parameters: 5x (2 min pulsed

ultrasound (1 s pulse, 1 s break), intensity 40/100; 30 s break). The insoluble fraction was then removed by centrifugation at 4°C, 9000 min^{-1} for 30 min, and glutathione Sepharose 4B (GE Healthcare) beads, equilibrated in washing buffer, were added to the supernatant (1 mL of settled, equilibrated beads per L of original bacterial culture). After 2 h, the beads were collected upon two rounds of centrifugation at 4°C, 4500 min^{-1} for 5 min and then washed five times with the buffer containing 50 mM Tris HCl pH 8.0, 100 mM NaCl, and 5 mM $MgCl_2$. Upon washing, the beads were resuspended in the equal volume of the washing buffer and incubated with Prescission protease at 4°C. Upon overnight incubation, the beads were centrifuged at 9000 rpm at 4°C to obtain clear, yellow eluate. The elution was repeated two more times with equal volume and the eluates were combined. A HiLoad Superdex 75 16/60 column (GE Healthcare) was equilibrated in buffer containing 10 mM Tris HCl pH 8.0 and 150 mM NaCl. Without a prior concentrating step, the eluate was then gel-filtrated and all fractions containing PYROXD1 were collected and pooled, concentrated using Amicon ultrafiltration units (Amicon Ultra centrifugal filter, MWCO 30 kDa, Merck), and subjected to the second round of gel filtration on the Superdex 75 16/60 column. Fractions containing PYROXD1 were collected and concentrated to the final concentration of 40 μmol·L^{-1}. The protein was then flash frozen in liquid nitrogen and stored at −80°C.

Cloning, purification and characterization of PYROXD1 variants

PYROXD1 variants N155S, Q372H, W376A, and H401A were generated by two-step overlap extension touch-up PCR, and then cloned into the pGEX-6P-1 vector.

All variants were expressed and purified as described for the WT protein. Ultraviolet-visible spectra of the variants (40 μm) for qualitative detection of FAD were performed at 25°C, using DeNovix spectrophotometer (DS 11 series) with 1 mm optical pathlength at 10 nm resolution.

Expression of recombinant selenomethionine PYROXD1

The pGEX-6P-1 encoding for GST-PYROXD1 was transformed into the *Escherichia coli* BL834 strain (Novagen) using LB medium and pre-culture was grown in the same medium overnight at37°C. Subsequently, bacteria were diluted into minimal medium, containing potassium-hydrogen phosphate (10.5 g·L^{-1}), potassium-dihydrogen phosphate (4.5 g·L^{-1}), ammonium-sulfate (1.0 g·L^{-1}), and sodium-citrate dihydrate (0.5 g·L^{-1}), 1 mM magnesium-sulfate, 20 μM thiamine, 40 mg·L^{-1} of all L-amino acids except methionine, and 0.2% (m/m) glucose supplemented with 40 mg·L^{-1} selenomethionine and grew until optical density (400 nm) reached 0.4. They were then collected, washed in minimal buffer containing potassium-hydrogen phosphate (10.5 g·L^{-1}), potassium-dihydrogen phosphate (4.5 g·L^{-1}), ammonium-sulfate (1.0 g·L^{-1}), and sodium-citrate dehydrate (0.5 g·L^{-1}) and resuspended in the minimal medium described above, without selenomethionine supplementation. The culture was then grown for 30 min, after which the medium was supplemented with selenomethionine (40 mg·L^{-1}), and grown again for 30 min, until the final optical density reached 0.5. The temperature was then dropped to 18°C and expression and purification were continued as described above.

Targeted metabolomics of FAD

The sample of recombinant PYROXD1 was diluted 1:10 with pure acetonitrile and injected onto a SeQuant ZIC-HILIC HPLC column (Merck, 100 × 2.1 mm; 5 μm) operated with an Ultimate 3000 HPLC system (Dionex, Thermo Fisher Scientific) and separated at a flow rate of 100 μl·min^{-1}. A 20 minute gradient (A: 90% acetonitrile 10% 10 mM aqueous ammonium acetate; B: 50% acetonitrile 50% 10 mM aqueous ammonium acetate) was used for separation. The HPLC was directly coupled to a TSQ a TSQ Vantage mass spectrometer (Thermo Fisher Scientific) via electrospray ionization. The following transition was used for quantitation in the negative ion mode (2.8 kV): FAD 784 *m/z* → 346 *m/z* with a collision energy setting of 40V (qualifier ions 181 *m/z* and 97 *m/z*). The identity of the compound was confirmed by the retention time of a chemically pure standard of FAD (Flavin adenine dinucleotide disodium salt hydrate, Sigma).

UV-visible spectroscopy

UV-visible spectroscopy measurements of the recombinant PYROXD1 was performed using Specord 200 plus spectrophotometer from Analytik Jena at 25°C and a quartz cuvette with 1 cm optical path length.

Extinction coefficient determination

To determine the extinction coefficient, UV-visible spectrum of the recombinant WT PYROXD1 (20 μM) was recorded at 25°C before and after FAD release through denaturation by 0.2% SDS and centrifugation. The extinction coefficient for PYROXD1 at 451 nm was then calculated based on the extinction coefficient of free FAD 11,300 $M^{-1}\cdot cm^{-1}$ (Macheroux, 1999).

Spectral characterization of PYROXD1 reduced by NADPH

Recombinant WT PYROXD1 (10 μM) was kept in a glove box from Belle Technology (Weymouth, UK) for 2 h to deoxygenate and transferred to a 1 cm quartz cuvette with airtight lid. A hanging drop of NADPH was applied at the bottom of the cuvette lid. After recording the spectrum of the oxidized protein as described above, the NADPH reduction reaction was initiated by inverting the cuvette, thereby mixing protein and NADPH. Spectra were then recorded every 16 s until no further change was observed, i.e., the charge transfer formation was completed. The final concentration of NADPH used was 9.5 μM. The cuvette was then opened to allow exposure to air and the reoxidation reaction with O_2 was performed in the same way. In a separate experiment, the NADPH

reduction was performed as described above, and a hanging drop of ubiquinone-1 (coenzyme Q1, Sigma) solution in ethanol was then used to initiate the oxidation reaction upon mixing. The final concentration of ubiquinone-1 in the cuvette was 20 μM.

Anaerobic photoreduction

For photoreduction, 10 μM PYROXD1 was deoxygenated as described above and transferred to a 1 cm quartz cuvette, and 5 mM EDTA, 2 μM 5-deazaFMN, and 4 μM benzyl viologen (Sigma) were added (final concentrations designated). The cuvette was then illuminated by a 10 W LED floodlight (Luminea) to reduce PYROXD1 through light exposure. Spectra were recorded until no further change could be observed. Afterward the cuvette was opened to allow air exposure and reoxidation by O_2 was performed in the same way.

Pre-steady state kinetics

Recombinant PYROXD1 (20 μM WT or N155S variant) was kept in a glove box (Belle Technology) with nitrogen atmosphere for 2 h to deoxygenate. The reaction buffer, composed of 50 mM tris-HCl pH 8.0, 50 mM NaCl, and 10 mM $MgCl_2$ was deoxygenated by flushing with nitrogen and overnight incubation in the glove box. The reductive half-reaction was measured upon mixing of PYROXD1 with equal volume of 2-30 mM NADPH (β-Nicotinamide adenine dinucleotide 2′-phosphate reduced tetrasodium salt hydrate, Merck) or NADH (β-Nicotinamide adenine dinucleotide, reduced disodium salt hydrate, Merck) solutions in the reaction buffer. Concentrations of stock solutions of NADPH and NADH were confirmed spectrophotometrically before use. The device used to perform the experiment was SF-61SX2 stopped flow (TgK Scientific Limited) placed in the glove box at 25°C. Absorbance changes were measured with a PM-61 s photomultiplier (TgK Scientific Limited) at 451 nm. Each measurement was performed in a technical triplicate and the observed rate constants were generated through exponential fitting in the kinetic studio software (TgK Scientific Limited). Final K_d and k_{red} values were calculated by the Prism8 software from GraphPad Prism using saturation fitting. Average values with standard deviation (σ = 0.05) were represented in the scatter graph.

Steady state measurements

Steady state oxidoreductase activities of PYROXD1 were measured using the following protocol: equal volumes (100 μL) of solution of NADPH (solution 1) and a solution of enzyme and the electron acceptor substrate (100 μL) (solution 2) were mixed and absorbance at 340 nm was measured using Synergy H1 Hybrid Multi-Mode Microplate Reader at room temperature. The assay buffer was 50 mM tris-HCl pH 8.0, 50 mM NaCl, and 5 mM $MgCl_2$. The final concentration of NADPH was 300 μM NADPH in all experiments. The final concentration of PYROXD1 was 42.3 mg·L^{-1} in the experiment comparing activities of variants and activities with different substrates, and 33.8 mg·L^{-1} in experiment comparing activities of oligomeric states. The final concentrations of electron acceptors were: Q1 70 μM (coenzyme Q1, Sigma), GSSG 500 μM (L-glutathione oxidized, Sigma), sodium-dehydroascorbate 300 μM ((L)-dehydroascorbic acid, Sigma), H_2O_2 200 μM (hydrogen peroxide 30%, Sigma), cystine 700 μM (L-cystine, Sigma), sodium-lipoate 400 μM ((±)-α-Lipoic acid, Sigma), and insulin 100 μM (Insulin, Human Recombinant, Sigma); monodehydroascorbate was generated *in situ* from sodium ascorbate (2 mM) ((+)-Sodium L-ascorbate, Sigma) and ascorbate oxidase (1 U·mL^{-1}) (Ascorbate Oxidase from *Cucurbita sp*., Sigma). Stock solutions of the electron-acceptors were prepared in water (GSSG, dehydroascorbic acid, H_2O_2), ethanol (Q1 and lipoic acid) and 100 mM HCl (cystine and insulin). Volume of the added stock solution never exceeded 2.5% of the reaction volume. Reaction mixtures without enzyme (enzyme replaced with gel-filtration buffer) and without electron-acceptor (electron acceptor replaced with corresponding stock solvent) were used as negative controls. Enzymatic activities were measured based on the slope of the absorbance decrease [min^{-1}], and using optical path 0.56 cm, reaction volume 0.2 mL and extinction coefficient 6220 M^{-1}·cm^{-1} to calculate the specific activity. One unit of activity was defined as the amount of enzyme that oxidizes 1 μM of NADPH in 1 min. All measurements were done at room temperature. Significance of average values for all samples was evaluated by comparing values obtained for the sample measurements with the values obtained for the corresponding control using t test assuming unequal variances, σ = 0.05.

Crystallization

PYROXD1 crystals were obtained using the sitting drop vapor diffusion method at 4°C. 100 nL of recombinant PYROXD1 (WT or selenomethionine-enriched protein, 5 mg·mL^{-1}) were mixed with 100 nL of reservoir solution containing 2 M ammonium-sulfate, 0.5 g·mL^{-1} PEG 400 (Polyethylene glycol 400, Sigma), 100 mM MES (MES hydrate, Sigma) pH 6.7, 100 mM lithium-acetate, and 5 mM TCEP (Tris(2-carboxyethyl)phosphine hydrochloride, Thermo Scientific) using Mosquito 3.10. (TTP Biotech). The crystals emerged after three days and reached full size until the sixth day. WT crystals were then dehydrated, through incubation with a series of seven solutions containing 100 mM MES pH 6.8, of PEG 400 (5%–40% in gradient), and ammonium-sulfate (2-0 M in a gradient) and afterward collected in cryo-protectant consisting of 27% (v/v) glycerol, 2 M ammonium-sulfate, 100 mM MES pH 6.5, 0.5 g·mL^{-1} PEG 400 with 5 mM TCEP. Ultimately, they were flash-cooled in liquid nitrogen. X-ray diffraction data were collected at the beamline MASSIF-3 at the ESRF (Grenoble, France). Anomalous diffraction data were processed at a wavelength of 0.9677 and scaled using the XDS package (Kabsch, 2010) to a resolution of 3.2 Å. Initial phases were obtained by Molecular Replacement using PHASER (McCoy et al., 2007)and the structure deposited under 4BV6 in the PDB as starting model (Ferreira et al., 2014). Phases was improved in iterative cycles of manual building with COOT (Emsley and Cowtan, 2004) using the anomalous signal of selenium to trace the amino acid sequence and automatic refinement with Phenix (Liebschner et al., 2019)omitting 5 % of randomly selected reflections

Please cite this article in press as: Asanović et al., The oxidoreductase PYROXD1 uses NAD(P)$^+$ as an antioxidant to sustain tRNA ligase activity in pre-tRNA splicing and unfolded protein response, Molecular Cell (2021), https://doi.org/10.1016/j.molcel.2021.04.007

for calculation of R_{free}. Model quality was monitored using MolProbity (Williams et al., 2018) and the final model exhibited good stereochemistry with 96 % of residues in favored regions of the Ramachandran plot and without any outliers.

DALI analysis

For comparison of PYROXD1 structure with the structures of related proteins, we uploaded our PYROXD1 model to DALI server (Holm, 2020). First, published structures with the highest similarity (z-score) to PYROXD1 were identified through a heuristic PDB search. Then, our model of PYROXD1 was 3D-superimposed with 17 related structures representing enzymes with different enzymatic activities, and including the following pdb entries: 3fg2, 2gqw, 4h4r, 5jcm, 5jci, 3kd9, 5voh, 5kvh, 2bc0, 1ebd, 4bv6, 5x1y, 6b4o, 6bu7, 2eq8, 3dk9, and 2zz0. Finally, the PYROXD1 structure was presented as α-C trace backbone and colored according to the sequence similarity between PYROXD1 and the homologs.

Native mass spectrometry

Prior to analysis, recombinant PYROXD1 was buffer-exchanged into 100mM ammonium acetate using Biorad Micro Bio-Spin P-6 Gel Columns. Native mass spectrometry experiments were carried out on a Synapt G2Si instrument (Waters, Manchester, UK) with a nanoelectrospray ionisation (nESI) source. Mass calibration was performed by a separate infusion of NaI cluster ions. Solutions were ionised through a positive potential applied to metal-coated borosilicate capillaries (Thermo scientific). Protein samples (5 μM) were sprayed from 100 mM ammonium acetate pH 6.8 with the following parameters; capillary voltage 1.3 kV, sample cone voltage 70 V, extractor source offset 40 V, source temperature 50°C. Data were processed using Masslynx V4.1 software.

Oligomerization assays and native PAGE

Oligomerization assays were performed using the following protocol: protein sample (WT or N155S PYRROXD1), final concentration of 6 μmol·L^{-1} was mixed with NAD(P)(H) (0.125, 0.25, 0.5, 1.25, 2.5, 5 mM) or H_2O_2 (0.025, 0.05, 0.1, 0.2, 0.4, 0.8, 1,6, 3.2 mM, final concentration) in total reaction volume of 5 μL. Additional components in the reaction mix included in the some experiments were tris(2-carboxyethyl)phosphine (TCEP, final concentration of 5 mmol·L^{-1}) or catalase (Catalase from bovine liver, Sigma, 0.3 U·mL^{-1}). The assay was done in a buffer containing 30 mM HEPES/KOH pH 7.4, 100 mM KCl, 5 mM $MgCl_2$, 40 mM AEBSF, 10% glycerol, 1% NP40. After all the components were mixed, the samples were incubated at 30°C for 3h. After completion of incubation, samples were mixed with the 2xNative gel loading dye (composed of 62.5 mM Tris-HCl, pH 6.8, 25% glycerol, and 1% Bromophenol Blue). The reaction products were separated on 10% Native polyacrylamide Gel (composed of 10%/0.27% Acrylamide/Bis-acrylamide (ProtoGel) and 150 mM Tris-HCl, pH = 8.8) using running buffer composed of 25 mM Tris base and 192 mM glycine, and detected by InstantBlue (Expedeon) staining.

Purification of PYROXD1 oligomeric states

PYROXD1 was expressed and a crude preparation was obtained as described above. Upon the first gel-filtration run, the fractions with theoretical molecular weights expected to cover the peaks of the dimeric and oligomeric PYROXD1 were collected, pooled and concentrated. The oligomeric states were then enriched through four further gel filtration steps on a HiLoad Superdex 75 16/600 column and HiLoad Superdex 200 16/600 column (GE Healthcare) in the same buffer at 4°C, resulting in monomer, dimer, oligomer and polymer/aggregate preparations. All preparations were concentrated to the final concentration of PYROXD1 active sites (bound FAD molecules) of 40 μmol·L^{-1}, flash frozen in liquid nitrogen and kept at −80°C.

Co-immunoprecipitation and mass spectrometry analysis

HEK293 cells expressing FLAG-PYROXD1 (see Experimental model and subject details – Cell lines) upon doxycycline induction and a control, untagged cell line, were treated with doxycycline (1 μg·L^{-1}) for 24 h. Cells were then harvested and lysed in a buffer containing 30 mM HEPES/KOH pH 7.4, 100 mM KCl, 5 mM $MgCl_2$, 40mM AEBSF, 10% glycerol, 1% NP40, and either 0.5 mM NADPH, 0.5 mM NADP$^+$ or no nucleotide. Anti-FLAG M2 Affinity Gel (Sigma) was added to the extracts and incubated on a rotating wheel at 4°C for 1 h for FLAG-PYROXD1 immunoprecipitation. Beads were then washed five times with the same buffer. Upon the final wash, beads were boiled in 5x SDS loading buffer, subjected to denaturing, reducing SDS-PAGE and detected using InstantBlue protein stain (Sigma). Afterward, entire lanes were cut from the gel. Immunoprecipitates comparing NADP$^+$ to buffer control were prepared in independent triplicates. The processing of the gel samples was done according to the protocol described in detail in Mair et al. (2015). Namely, gel pieces were cut and washed in ammoniumbicarbonate/acetonitrile buffer. Disulphide bridges were reduced with dithiothreitol (DTT) and free thiols alkylated with iodoacetamide (IAM). After tryptic digestion peptides were extracted from the gel by sonication. The peptide solutions were desalted on custom-made C18 StageTips. Peptide samples were separated on an Ultimate 3000 RSLC nano-flow chromatography system, using a pre-column for sample loading (PepMapAcclaim C18, 2 cm × 0.1 mm, 5 μm) and a C18 analytical column (PepMapAcclaim C18, 50 cm × 0.75 mm, 2 μm; all Thermo Scientific Dionex), applying a linear gradient from 2 to 35% solvent B (80% acetonitrile, 0.1% formic acid; solvent A 0.1% formic acid) at a flow rate of 230 nl/min over 120 minutes. Eluting peptides were analyzed on a Q Exactive HF-X Orbitrap mass spectrometer (Thermo Scientific). For the data-dependent mode survey scans were obtained in a mass range of 375–1,500 m/z with lock mass on, at a resolution of 120.000 at 200 m/z. The AGC target value was 3E6 with a maximal injection time of 60 ms. The 8 most intense ions were selected with an isolation width of 1.6 Da and 0.2 Da isolation offset, fragmented in the HCD cell at 28% collision energy and the spectra recorded at a target value

of 1E5 with the maximal injection time of 250 ms and a resolution of 30000. Peptides with unassigned charge state, a charge of +1 or > +6 were excluded from fragmentation, the peptide match and exclude isotope features were enabled and selected precursors were dynamically excluded from repeated sampling for 30 s. Data were processed and analyzed as described in Quantification and statistical analysis – Mass spectrometry data analysis.

Recombinant expression and purification of StrepII-GFP-RTCB

DNA encoding human RTCB was cloned into the UC Berkeley MacroLab 438-Rgfp vector (gift from Scott Gradia, Addgene plasmid #55221). The fusion protein containing an N-terminal StrepII-GFP tag was expressed as described above for the tRNA ligase complex. The clarified lysate from 3 L of Sf9 cell culture was applied to a gravity column containing 5 mL Strep-Tactin resin (IBA). The column was washed with buffer containing 20 mM HEPES pH 8.0, 500 mM KCl, 1 mM DTT, and 2 mM $MgCl_2$ and bound protein was eluted with the wash buffer supplemented with 2.5 mM desthiobiotin. The protein was concentrated using a centrifugal filter (Amicon Ultra, MWCO 10 kDa, Sigma) and further purified by size-exclusion chromatography (Superdex 200, GE Healthcare), eluting with buffer containing 20 mM HEPES pH 8.0, 500 mM KCl, 2 mM $MgCl_2$, and 1 mM DTT. Fractions containing StrepII-GFP-RTCB were pooled, concentrated to 2.2 mg·mL^{-1} using a centrifugal filter (Amicon Ultra, MWCO 10 kDa, Sigma), flash frozen in liquid nitrogen and stored at −80°C.

In vitro pull-down assay

0.2 nmol of StrepII-GFP-RTCB was diluted in 200 μL of reaction buffer containing 20 mM HEPES pH8.0, 150 mM KCl, 0.1% Tween-20, 1 mM NADPH/NADP$^+$/NADH/NAD$^+$, supplemented with 5 mM $MgCl_2$, as indicated. This solution was incubated by gently rocking for 30 min at 4°C with 2 μL (packed volume) of MagStrep "type 3" XT beads (IBA). The supernatant was removed and the beads were washed twice with 500 μL of reaction buffer. 0.4 nmol of PYROXD1 in 200 μL of reaction buffer was added to the washed beads and incubated gently by rocking for 30 min at 4°C. The supernatant was removed and the beads were washed three times with 500 μL of reaction buffer. After removal of the final wash, the beads were resuspended in 40 μL of 1x SDS loading dye (45 mM Tris pH 6.8, 10% glycerol, 1% SDS, 50 mM DTT, 0.002% bromophenol blue). The samples were incubated at 95°C for 5 min and 8 μL of the sample was resolved on a 4%–15% Mini-PROTEAN® TGX Precast Gel (Biorad) and stained with Coomassie blue dye.

Recombinant expression and purification of the tRNA ligase complex

Upon culturing for 60 h (see Experimental model and subject details – Expression systems), insect cells were resuspended in lysis buffer (20 mM HEPES pH 8.0, 150 mM NaCl, 0.1 % Tween-20, cOmplete Protease Inhibitor Cocktail (Roche)), and lysed by sonication. The lysate was clarified by centrifugation for 30 min at 30.000 g at 4°C. The supernatant was applied to a Ni-NTA Superflow resin (QIAGEN) and eluted with buffer containing 20 mM HEPES pH 8.0, 500 mM NaCl, 0.5 mM TCEP, and 250 mM imidazole. The fusion tags were removed by proteolysis using His6-tagged Tobacco Etch Virus (TEV) protease during an overnight dialysis at 4°C against 20 mM HEPES pH 8.0 and 150 mM NaCl. The protein solution was subsequently supplemented with 0.5 mM TCEP and applied to a Ni-NTA Superflow resin (QIAGEN) to remove any uncleaved protein, His_6-TEV protease, and remaining impurities. The complex-containing flow-through and wash fractions were concentrated using a centrifugal filter (Amicon Ultra, MWCO 30 kDa, Sigma), loaded onto a size-exclusion chromatography column (Superdex 200, GE Healthcare) and eluted in buffer containing 20 mM HEPES pH 8.0, 150 mM KCl, and 0.5 mM TCEP. Peak fractions containing the tRNA ligase complex were concentrated to 9.4 mg ml^{-1} using a centrifugal filter (Amicon Ultra, MWCO 30 kDa, Sigma), flash frozen in liquid nitrogen and stored at −80°C.

Recombinant expression and purification of RTCB

Upon culturing for 60 h (see Experimental model and subject details – Expression systems), insect cells were lysed by sonication in buffer containing 20 mM Tris pH 8.0, 150 mM NaCl, 5 mM imidazole, 0.1% Tween 20, and cOmplete Protease Inhibitor Cocktail (Roche). The lysate was clarified by centrifugation for 30 min at 30.000 g at 4°C. The supernatant was applied to a Ni-NTA Superflow resin (QIAGEN) and eluted with buffer containing 20 mM Tris pH 8.0, 500 mM NaCl, and 250 mM imidazole. The fusion tag was removed by a His_6-tagged TEV protease during an overnight dialysis at 4°C against buffer containing 20 mM HEPES pH 8.0, 500 mM KCl, and 3 mM $MgCl_2$. The dialyzed protein mixture was passed through a Ni-NTA Superflow resin (QIAGEN) to remove the His_6-TEV protease, remaining impurities and uncleaved protein. The RTCB-containing fractions were concentrated using a centrifugal filter (Amicon Ultra, MWCO 10 kDa, Sigma) and purified by size-exclusion chromatography (Superdex 75, GE Healthcare) in buffer containing 20 mM HEPES pH 8.0, 500 mM KCl, 3 mM $MgCl_2$, and 1 mM DTT. RTCB-containing fractions were pooled, concentrated to 6.6 mg·ml^{-1} using a centrifugal filter (Amicon Ultra, MWCO 10 kDa, Sigma), flash frozen in liquid nitrogen and stored at −80°C.

Recombinant expression and purification of Archease

Upon expression, bacterial cells (see Experimental model and subject details – Expression systems) were lysed in 20 mM Tris pH 8.0, 500 mM NaCl, and 5 mM imidazole and the lysate was clarified by centrifugation for 30 min at 20.000 g at 4°C. The clarified lysate was applied to two 5 mL Ni-NTA Superflow cartridges (QIAGEN); the resin was washed with buffer containing 20 mM Tris pH 8.0, 500 mM

NaCl, and 10 mM imidazole and bound protein was eluted with buffer containing 20 mM Tris pH 8.0, 500 mM NaCl, and 250 mM imidazole. The fusion tag was removed with His_6-tagged TEV protease during an overnight dialysis at 4°C against 20 mM Tris pH 8.0, 250 mM KCl, and 5% glycerol. The sample was subsequently re-applied onto the Ni-NTA Superflow cartridges to remove the affinity tag and His_6-TEV protease. The flow-through fraction was concentrated using a centrifugal filter (Amicon Ultra, MWCO 10 kDa, Sigma) and purified by size-exclusion chromatography (Superdex 75, GE Healthcare), eluting with buffer containing 20 mM HEPES pH 7.5, 250 mM KCl, and 1 mM DTT. Archease-containing peak fractions were concentrated to 43 mg·ml^{-1} using a centrifugal filter (Amicon Ultra, MWCO 10 kDa, Sigma), flash frozen in liquid nitrogen and stored at −80°C.

Generation of human RTCB model

To generate a model of human RTCB, sequence of human RTCB was uploaded to Swiss-model and the homology model was built based on the 1.48 Å structure of the non-guanylated RTCB from *Pyrococcus horikoshii*, PDB entry 4dwr, Swiss-model template 4dwr.1.A. (Bienert et al., 2017; Guex et al., 2009; Waterhouse et al., 2018).

In vitro reconstitution system experiments

For the *in vitro* reconstitution of the redox-regulation of the tRNA-LC, we used the following two-part approach: first, the recombinant tRNA-LC (25 nM) or RTCB (25 nM) and Archease (200 nM) were pre-incubated with a concentration gradient of H_2O_2 in the buffer containing 30 mM HEPES/KOH pH 7.4, 100 mM KCl, 5 mM $MgCl_2$, 40mM AEBSF, 10% glycerol, and 1% NP40; then, the pre-incubation was stopped by TCEP-containing reaction cocktail (described above, 2/3, v/v) and the activity of the tRNA-LC was measured using the RNA ligation (circularization) assay. In different experiments, one or combination of the additional compounds was added to the system during pre-incubation: TCEP (0.5 mM), NADP(H) (0.5 mM), BCS (100 μM), Q1 (100 μM), and PYROXD1 (WT, variants or purified oligomeric states, 130 nM). For the experiment assessing the rescue rather than the prevention of the inactivation of the tRNA-LC, PYROXD1 was added upon pre-incubation. For the experiment with heat-denatured PYROXD1, the enzyme was boiled for 3 min and centrifuged at 13.000 rpm for 10 min. For the long-term O_2-exposure experiment, the tRNA-LC and Archease were incubated for 6 days at 20°C in the solution of 10 μL and shaken at 60 min^{-1}, and the tubes were opened once a day to allow exchange of the air in the tubes with the fresh air. For all *in vitro* reconstitution experiments, the buffer was prepared at least one day in advance, using deionized water (resistance of roughly 18.5 MΩ) and aliquoted with glass pipette to avoid metal ion contamination from the plastic tips; the buffers were stored at 4°C for not longer than a month.

For the experiments with metal ions, the buffer containing 30 mM HEPES/KOH pH 7.4, 100 mM KCl, 40mM AEBSF, 10% glycerol, and 1% NP40 was incubated with Chelex 100 sodium form (Sigma) chelating resin (50 mg·mL^{-1}) for 1 h, at 4°C, rotating at 18 min^{-1}. After that, the resin was removed by centrifugation and the buffer was supplemented with $MgCl_2$ and pH was readjusted to match the pH of the untreated buffer that was used in other reconstitution experiments. Trace metal ion salts used for the metal supplementation experiments are copper(II)-sulfate pentahydrate (Fluka), iron(II)-chloride (Sigma), iron(III)-sulfate monohydrate (Sigma), zinc-chloride (Sigma), and manganese(II)-sulfate monohydrate (Fluka) at the designated final concentration.

Dimedone labeling of sulphenic acids

For detection of cysteine oxidation in recombinant tRNA-LC components and PYROXD1, the dimedone-based sulphenic acid labeling strategy was used (Seo and Carroll, 2009). All experiments were performed using a buffer containing 30 mM HEPES/KOH pH 7.4, 100 mM KCl, 5 mM $MgCl_2$, 40mM AEBSF, 10% glycerol, 1% NP40, and the final concentration of dimedone of 1 mM. In PYROXD1 experiments, recombinant PYROXD1 (6 μM) was incubated with dimedone and with either H_2O_2 or NADPH under the conditions described for the oligomerization experiments. For experiments using the tRNA-LC or RTCB, the recombinant proteins (at 100 nM), were incubated with dimedone and H_2O_2 under conditions described for the incubation period of *in vitro* reconstitution experiments. In all cases, the labeling reaction was terminated by the addition of the reducing 5xSDS loading dye. Proteins were then subjected to reducing, denaturing SDS-PAGE and dimedone-sulphenic acid adducts were detected by Western Blotting as described above.

Biotin-NAD pulldown assay

Magnetic Dynabeads M-280 Streptavidin (Thermo Fisher) were equilibrated in a buffer containing 30 mM HEPES/KOH pH 7.4, 100 mM KCl, 5 mM $MgCl_2$, 40mM AEBSF, 10% glycerol, 1% NP40. Subsequently, beads were resuspended either in the same buffer or in the same buffer enriched with 20 μM biotinylated-NAD$^+$ (Trevigen). The beads were then washed with the buffer and resuspended in the same buffer containing recombinant tRNA-LC either with or without 1 mM soluble NAD(P)(H). Upon 1 h incubation (4°C, 18 min^{-1}), the beads were separated using DynaMag-5 Magnet holder (Thermo Fisher) and the remaining solution was discarded. The tubes still being fixed in the holder, the beads were washed four times with the same buffer as fast as possible and without being resuspended, to enable washing, but preventing the dissociation of the bound protein into the washing buffer. The beads were then resuspended in 2xSDS loading buffer and analyzed by western blotting as described above.

Please cite this article in press as: Asanović et al., The oxidoreductase PYROXD1 uses NAD(P)$^+$ as an antioxidant to sustain tRNA ligase activity in pre-tRNA splicing and unfolded protein response, Molecular Cell (2021), https://doi.org/10.1016/j.molcel.2021.04.007

Molecular dynamics simulations

System preparation

PYROXD1 X-ray structure was pre-processed using Modeler 9.21 software (Fiser et al., 2000) for filling missing loops and atoms in sidechains. Non-missing residues were considered frozen using this protocol. The large missing loop (Lys196 – Ser 252) was approximated using an insertion composed of 6 Gly residues. Protonation states of residues were determined using PROPKA 3.0 (Olsson et al., 2011) under PDB2PQR 2.0.0 server (Dolinsky et al., 2007).

Initial docking

Docking runs were performed using GOLD software v. 5.6.0 (Jones et al., 1997). The ligand (NADPH) was prepared extracting coordinates from X-ray structure of the homolog protein (PDB:3CGE) and subsequently optimizing geometry in Gaussian09 at B3LYP/6-31G* level of theory (Gaussian 09, Revision A.02, (Frisch et al., 2009)). The binding site was defined as all residues present in a radius of 15Å around residue Gly156. Residue Gly156 was chosen according to homolog analysis and due to its proximity to the flavin group of the FAD molecule. Additionally, this residue represents part of the sequence previously identified through bioinformatic analysis as fingerprint of phosphate-binding site in NADP-binding proteins (Class I in NADP binding proteins) (Wu et al., 2012). The number of genetic algorithm runs was set to 50 per ligand, and 200% search efficiency was used. CHEMPLP scoring function (Korb et al., 2009) was used and docking was ran without early termination. All results were selected for analysis according to at least one of following criteria: Overall docking score have to be relatively high; the nicotinamide group of NADP should be reasonably close to the flavin group of the FAD molecule in order for the redox process to occur; the orthophosphate moiety of NADPH should interact with the phosphate-binding site. As a part of preliminary testing on the X-ray structure, docking runs were also performed with residues Lys176 and Phe184 defined as flexible.

Preliminary molecular dynamics

Preliminary Molecular Dynamic runs were used to access stability of the studied systems and to explore conformational fluctuations around the binding pocket accessible by plain-MD. Two systems were simulated: PYROXD1/FAD and PYROXD1/$FADH_2$. The PYROXD1/$FADH_2$ system was prepared by manual addition of hydrogens. The rest of the systems preparation process is explained in the Plain molecular dynamics (MD)section. Ensembles of PYROXD1/FAD and PYROXD1/$FADH_2$ conformations generated through MD were analyzed by molecular docking of NADPH and NADP$^+$, respectively. More details on the ensemble docking protocol are provided below.

Well-tempered metadynamics simulations

Since preliminary MD runs failed to improve docking results, most likely due to insufficient sampling of MD, an enhanced sampling algorithm for simulations – WTmetaD was used in further experiments. Metadynamics is a powerful enhanced sampling method intended for studying rare events by pushing the simulated system from local free-energy minima. Namely, metadynamics accelerate transitions between metastable states of studied system using the history dependent biasing potential applied on one or more collective variables (CV). In one of the most popular variants of metadynamics, well-tempered metadynamics (WTmetaD), the temperature tuning factor controls the sampling in CV space ensuring smooth convergence of the bias potential (Bussi and Laio, 2020). To enhance sampling of conformations of PYROXD1 relevant for NADP$^+$ or NADPH binding (with no intentions to obtain converged free-energy profiles), two independent WTmetaD runs (PYROXD1/$FADH_2$ and PYROXD1/FAD) were simulated for 2x50 ns each. As a starting conformation, we used the last conformations from preliminary MD runs for both systems. All WTmetaD runs were performed in PLUMED 2.3.5 (Tribello et al., 2014) patched to the GROMACS 2016.6 (Pronk et al., 2013). As a collective variable, the pocket radius of gyration was used. Pocket atoms were defined using residues positioned in radius of 4Å around the most populated poses selected in preliminary docking runs, excluding FAD/$FADH_2$ and residues positioned on the other side of FAD/$FADH_2$. Putative binding pocket residues included: Gly154, Asn155, Gly156, Gly157, Ala159, Lys176, Asp177, Asn182, Thr183, Phe184, Cys261, Glu262, Val263, Thr317, Gly318, Val319, Thr320, Met373, Arg374, Leu375, and Trp376. The bias factor for well-tempered metadynamics was set to 10. Hills were added every 2 ps, width of Gaussian hills was set to 0.1Å, while height was 0.6 kcal/mol. The temperature was set to 310 K. Conceptually similar methodology have been published recently (Basciu et al., 2019).

Ensemble docking of NADP$^+$/NADPH into generated conformations of PYROXD1

Acquired conformational ensembles of PYROXD1/$FADH_2$ and PYROXD1/FAD complexes during WTmetaD (or preliminary MD) were aligned using backbone atoms. NADP$^+$/NADPH respectively, were docked into each conformation according to protocol described above, in initial docking runs. No residues have been kept flexible. In house script was used to automate molecular docking runs. Top scored poses for both systems (PYROXD1/FAD/NADPH and PYROXD1/$FADH_2$/NADP$^+$) were selected for plain molecular dynamics runs to access overall stability and exclude complexes that represents metastable states.

Plain molecular dynamics (MD)

MD simulations were performed using GROMACS 2016.6 software (Pronk et al., 2013). Initial coordinates were retained from top-scored complexes obtained through ensemble molecular docking. PYROXD1/$FADH_2$ system was simulated after manual addition of hydrogens on obtained X-ray structure of PYROXD1/FAD. Each system was subjected to extended minimization and equilibration protocol. The AMBERff14SB (Maier et al., 2015) force field was used for generation of protein topology. NADP$^+$ and NADPH parameters were acquired from Amber parameters database (http://amber.manchester.ac.uk). The cofactors FAD and $FADH_2$ were parameterized with the xLeap module of AmberTools (Case et al., 2018) employing the general Amber force field (GAFF2) (Vassetti et al., 2019). The atomic charges of previously optimized structures of FAD and $FADH_2$ (B3LYP/6-31G*) were fitted on the electrostatic potential (RESP) obtained at the HF/6-31G* level of theory with GAUSSIAN09 (Gaussian 09, Revision A.02, (Frisch et al., 2009)). The

protein-ligand complexes were solvated with the TIP3P water model, and neutralized with Na^+ counterions in an octahedral periodic box. Systems were minimized with steepest descent algorithm with maximum force set to 10 kJ mol^{-1} nm^{-1} and 5000 steps. Subsequent equilibration of the systems was performed first in NVT ensemble for 250 ps at 310 K using Nosé–Hoover thermostat (Evans and Holian, 1985). Second, equilibration in NPT ensemble was performed maintaining the pressure at 1.0 bar with Parrinello-Rahman barostat (Parinello, 1981). All atom position restrains were applied on protein atoms, while the solvent molecules and counterions were unrestrained. Position restraints were gradually removed using force constants of 1000, 100, and 10 kJ/mol nm^{-2}. Each NPT equilibration step was performed for 500 ps of simulation. Finally, two replicas of 100 ns simulations were performed for each system, with 2 fs timestep in NPT ensemble. Each replica was started using different random seed velocity to alleviate sampling. Particle Mesh Ewald (PME) approach for calculation of long-range electrostatic using grid spacing of 0.12 Å was used, while 10 Å non-bonded cut-off values were used for Coulomb and Van der Walls interactions. LINCS algorithm was used for all bonds constrains. Trajectories were analyzed using Gromacs built-in tools.

QUANTIFICATION AND STATISTICAL ANALYSIS

Statistical tests

To assess statistical significance in mouse experiments (heart weight, ejection fraction), mRNA expression (qPCR), kinetic measurements (steady-state and pre-steady state kinetics), we used unpaired Student's t test assuming unequal variances, with *, $p < 0.05$; **, $p < 0.01$; ***, $p < 0.005$. For mass spectrometry analysis, Benjamini-Hochberg correction for p values was applied (see below).

Mass spectrometry data analysis

Raw data were processed using the MaxQuant software package 1.6.0.16 (https://www.maxquant.org/) searching against the human Uniprot reference database, the protein sequences of the constructs and a custom-made database of common contaminants. The search was performed with full tryptic specificity and a maximum of two missed cleavages. Carbamidomethylation of cysteine residues was set as fixed, oxidation of methionine and N-terminal protein acetylation as variable modifications—all other parameters were set to default. The match between run feature and the search for 2nd peptides was enabled. Results were filtered at protein and peptide level for a false discovery rate of 1%. The protein groups table was imported into Perseus 1.6.6.0, reverse hits and contaminants were filtered out as well as hits with less than 2 valid LFQ values in at least 1 experimental group. Missing LFQ values were imputed by values from a normal distribution. Data were statistically analyzed with LIMMA. To determine enriched proteins statistical analysis was performed in R (R Development Core Team, 2019) using the limma package (Ritchie et al., 2015) and applying the Benjamini-Hochberg correction for p values. The mass spectrometry proteomics data have been deposited to the ProteomeXchange Consortium via the PRIDE (Perez-Riverol et al., 2019) partner repository with the dataset identifier PXD018831.

Image quantification

To quantify band intensities in autoradiography images, we used ImageQuant software, and substrate conversion rate was calculated as the quotient of the substrate and the sum of substrate and product band intensities.